The influence of vegetation index thresholding on EO-based assessments of exposed soil masks in Germany between 1984 and 2019

Zepp, Simone*, Jilge, Marianne, Metz-Marconcini, Annekatrin, Heiden, Uta

* corresponding author: Simone Zepp; simone.zepp@dlr.de; German Aerospace Center (DLR), Muenchener Str. 20, 82234 Wessling, Germany

Abstract

Knowledge about the spatial and temporal distribution of exposed soils is necessary for e.g., soil erosion mitigation. Earth Observation (EO) is a valuable data source for detecting exposed soils on a large scale. In the last couple of years, the multitemporal compositing technique has been used for the generation of so-called exposed soil composites that overcome the limitation of temporarily coverage of the soils with vegetation as it is occurring at agricultural sites. The selection of exposed soil pixels from the stack of multispectral images is mainly done using spectral reflectance indices such as NDVI, NBR2 and others calculated on a per-pixel basis. The definition of the thresholds that are applicable to large areas such as regions, countries or continents is still a challenge and requires a reliable and robust sampling data base. In this study, the Soil Composite Mapping Processor (SCMaP) is used to build exposed soil masks containing all pixels in a given time period showing at least once exposed soil. For this purpose, a modified vegetation index (PV) based on the NDVI is used to separate the soils from other land cover (LC) classes by two PV thresholds. The overall goal of this study is to derive and validate exposed soil masks from multi-year Landsat data stacks for Germany from 1984 to 2019. The first focus is set on the impact of a newly developed sampling approach of LC classes such as urban areas, deciduous forests and agricultural fields that are automatically derived from Corine Land Cover (CLC) data. The spectral-temporal behavior of these LC classes in $PV_{min/max}$ index composites show larger variability of the PV values compared to a manual sampling for selective LC classes such as urban areas. It reveals that the threshold definition method previously developed by Rogge et al. (2018) is not robust enough and the percentile rule used to define the T_{max} threshold had to be adapted from 0.995 to 0.900. On the other hand, the sampling data base has proven to be robust across time and region. The second focus of the paper is to validate all generated exposed soil masks covering Germany for seven time periods from 1984 to 2019. A linear correlation analysis was performed comparing the SCMaP data with surveys from the Federal Statistical Office (Destatis) and the CLC inventories. The comparison with both datasets showed high regression coefficients (R^2 = 0.79 to 0.90) with small regional deviations for areas in the Northern part of Germany. Strong correlation was found for time periods based on a higher number of cloud free Landsat images such as from 2000 to 2009. This demonstrates the high potential of SCMaP's to generate exposed soil masks based on an automated sampling and a robust threshold derivation. To contribute to soil erosion studies that need information about where and when soils are bare, accurate exposed soil masks in suitable time periods can be of great value.

Keywords: soil exposure, soil reflectance composites, Landsat, multispectral, thresholding

1. Introduction

Soils provide numerous ecosystem services that are essential for human life on Earth (Adhikari and Hartemink 2016). Knowledge about the spatial and temporal distribution of exposed soils is very informative for assessing ecosystem processes and statistical analyses and can serve as a basis for further soil-related assessments (Lavelle et al. 2014). Natural or anthropogenically induced soil degradation and erosion affects the quality of ecosystem services (Demattè et al. 2018). In particular, exposed soils that are not covered by vegetation are prone to erosion (Virto et al. 2015), resulting in a notable amount of soil loss each year (Borelli et al. 2017, Borelli et al. 2018, Steinhoff-Knopp and Burkhard 2018). In addition to the location and exposition of uncovered soils (Panagos et al. 2014 b, Panagos et al. 2015 b), the duration of exposure indicates the vulnerability of an area (Cerdan et al. 2010, Panagos et al. 2014 a) to different geofactors, such as wind (Borelli et al. 2015, Schmidt et al. 2017) or water (Gobin et al. 2004, Steinhoff-Knopp and Burkhard 2018). Thus, information on the spatial and temporal distribution of exposed soils enables estimations of the vulnerability of a region (Cerdan et al. 2010, Panagos 2015 a) and can support the assessment of the future availability of soil-derived ecosystem services (Baude et al. 2019).

Earth Observation (EO) is a valuable data source for detecting exposed soils. Merging information from multiple images have been developed as a suitable technique for many purposes such as cloud-free images (Hermosilla et al. 2015), crop and land cover (LC) detection (White et al. 2014, Griffiths et al. 2019, Hansen et al. 2011) and for analyzing forests (Adams et al. 2020). In the last couple of years, the compositing technique has also been used for the generation of images containing reflectance values of exposed soils (Rogge et al. 2018, Demattè et al. 2018, Diek et al. 2017, Vaudour et al. 2021). This is an important step towards subsequent large-scale soil analyses that overcomes the temporarily coverage of soils by vegetation. The selection of exposed soil pixels from the multitemporal time stack is still a challenge and there are different solutions tested by previous studies. Loiseau et al. (2019) empirically defined a threshold based on the Normalized Difference Vegetation Index (NDVI) to select exposed soil pixels. Demattè et al. (2018) used field soil samples spectrally measured in the laboratory to define a suitable NBR2 threshold for exposed soil compositing. The methodology was developed for an area-wide automated processing to retrieve soil spectral reflectances (Geospatial Soil Sensing System (GEOS3)). Diek et al. (2017) used the Bare Soil Index (BSI) to build a bare Soil Composite for top-soil characterization of the agricultural areas in Switzerland. Different indices (NDVI, NBR2, BSI and soil surface moisture index (S2WI)), thresholds and regulations for creating composites were tested and compared by Vaudour et al. (2021) for two test sites in France. In all these cases, exposed soils can be successfully separated from photosynthetic active vegetation. Spectral index thresholds are used due to its simplicity and applicability.

A lot of emphasis has been put to cope with the spectral similarity of soils with non-photosynthetic active vegetation (NPV; Daughtry, 2006) such as grasslands (dry condition) or deciduous forests (leaf-off condition). But also crop residuals can have an impact on the soil pixel purity. The clear spectral separation of NPV and exposed soils is hampered by the limited spectral resolution of multispectral images in the SWIR region (Asner and Heidebrecht 2001, Okin 2007, Demattè et al. 2018, Malec et al. 2015). However, studies from Demattè et al. (2018) and Rogge et al. (2018) have shown that this influence can be minimized. Demattè et al. (2018) have tested different NBR2 values in order to minimize the influence of NPV in the soils spectra that especially are traced back to stubbles and crop residuals. They concluded that the results can be improved, if longer time ranges are considered that allows for a stricter threshold and thus, purer bare soil pixels in the soil mask. Rogge et al. (2018) developments have focused on a clearer separation from grasslands and leaf-off conditions of deciduous forests. The developed technique uses the change of agricultural fields from soil exposure to vegetation coverage to derive two spectral index-based thresholds. The definition of these thresholds is based on LC classes derived from CORINE Land Cover (CLC) data sets that do not change in the observation period. Thus, the spectral-temporal behavior of urban areas, deciduous trees and agricultural fields are analyzed to set the thresholds. These thresholds are applied to first, separate exposed soils from permanently photosynthetic active vegetation and second, to distinguish between exposed soils and permanently non-vegetated areas such as urban areas, water and mine sites. In the result, only areas with a changing cover and an index value lower than a previously defined threshold are selected as exposed soils (exposed soil mask) and averaged (mean) into a soil reflectance composite. The advantage of this technique is that no further ancillary data is necessary to separate exposed soils from other LC classes such as forests and urban areas (e.g. Diek et al. 2017).

CLC are selected for the derivation of thresholds because it is European-wide available and thus, has the potential to derive thresholds suitable for continental processing. However, sampling of CLC pixels in Rogge et al. (2018) has been done manually, which is very time consuming and a pixel selection might not represent the spectral and spatial variability of the LC. For country-wide and continental mappings of exposed soils, automated sampling strategies are needed that first, can help to handle regional differences of LC dynamics (Ying et al. 2017) represented in multispectral satellite data and second, allows for repeated derivation of thresholds in order to analyze their stability across time. The influence of these parameters is not yet fully understood or analyzed. For operational processors such as SCMaP and GEOS3, it is important to know the effect of different threshold settings to optimize operational processors and find the best solution for the regions of interest.

The overall goal of this study is to derive and validate masks that contain exposed soil pixels from multi-year Landsat data stacks for Germany from 1984 to 2019. For the exposed soil masks, it is important to clearly separate grasslands in dry conditions and deciduous trees as examples for NPV from exposed soils. The first focus is set on the impact of the sampling strategy to derive spectral index thresholds. We use SCMaP for the detection of exposed soils that require two spectral index thresholds and we also used the concept of threshold definition based on percentile rules. For the definition of the threshold, this paper presents a new and fully automated sampling strategy. In order to analyze the impact of the sampling scheme, we compared the results of the automated sampling with the manual sampling (Rogge et al. 2018) by comparing the spatial-temporal behavior of the LC classes. Further, selection criteria such as the number of samples and the repeatability of the results are analyzed. We also tested, if the threshold definition rule that is used in Rogge et al. (2018) is still applicable. Therefore, the impact of the new sampling data base on the resulting exposed soil masks is analyzed. We select the best approach for deriving seven exposed soil masks for entire Germany for different time periods ranging between 1984 and 2019.

The second focus of the paper is to validate all exposed soil masks covering Germany for all time periods. For this objective, the selection of suitable and independent data sets that contain country-wide repeated statistics is essential. In Germany and regions with similar climate conditions, exposed soils are rare and occur predominantly in agricultural areas. The pixels that SCMaP is collecting for the exposed soil masks are characterized by a change from vegetated to non-vegetated condition. The majority of these pixels are occurring on agricultural sites. All other permanently vegetated and permanently non-vegetated areas are neglected. Therefore, we used two independent data sets that contain information on the coverage of agricultural areas at different time steps. The Federal Statistical Office (Destatis) collects statistical data regarding agricultural areas and crop types in Germany on a regular basis (Destatis 2017). However, determining the methods used for the data collection is in the responsibility of each federal state and might result in regional differences. For that purpose and for future continental processing, we additionally used the agricultural classes of the CLC surveys for the validation of exposed soil masks. Both data sets have their pros and cons and validation results are shown.

2. Study Area

Germany stretches over an area of 357,095.89 km², of which 47% is used for agricultural purposes (Destatis 2020 a). These areas are split into permanent grassland (14%) and cropland (33%). In order to discuss the regional differences of the developments in this study, a brief introduction to the characteristics of the federal states of Germany is necessary. Intensively used arable land is the dominant land use in the federal states of Schleswig-Holstein (41%), Lower Saxony (39%), North Rhine Westphalia (31%), Brandenburg (35%), Mecklenburg Western Pomerania (47%), Saxony (39%), Saxony-Anhalt (49%) and Thuringia (38%) (Destatis 2020 a, Destatis 2020 b). The federal states of Schleswig Holstein (22%), Lower Saxony (15%), Bremen (17%) and Saarland (16%) show a higher portion of permanent grasslands compared to the areas in the state. In particular, northern Germany is primarily covered by permanent grasslands.

The investigation area of Germany is covered by three bio-geographical regions (EEA 2016). These bio-geographical regions were developed by the European Environmental Agency (EEA) and represent similar biodiversity and biological structures based on comparable vegetation and climatic conditions (EEA 2016). All of Europe consists of eleven regions, which are defined geographical reference units for characterizing the habitat types and species present in different countries (EEA 2020). Germany is mainly covered by the continental bio-geographical region (Figure 1). Small portions in northwestern Germany are associated with the atlantic bio-geographical region, whereas the high mountainous areas in southern Germany are classified as an alpine bio-geographical region (EEA 2016).

Multiple analyses on the influence of thresholding on the derivation of the exposed soil masks shown in this study are performed for five subportions of the study area (Figure 1). The test areas were selected to cover all three bio-geographical regions and land cover/land use types in Germany.

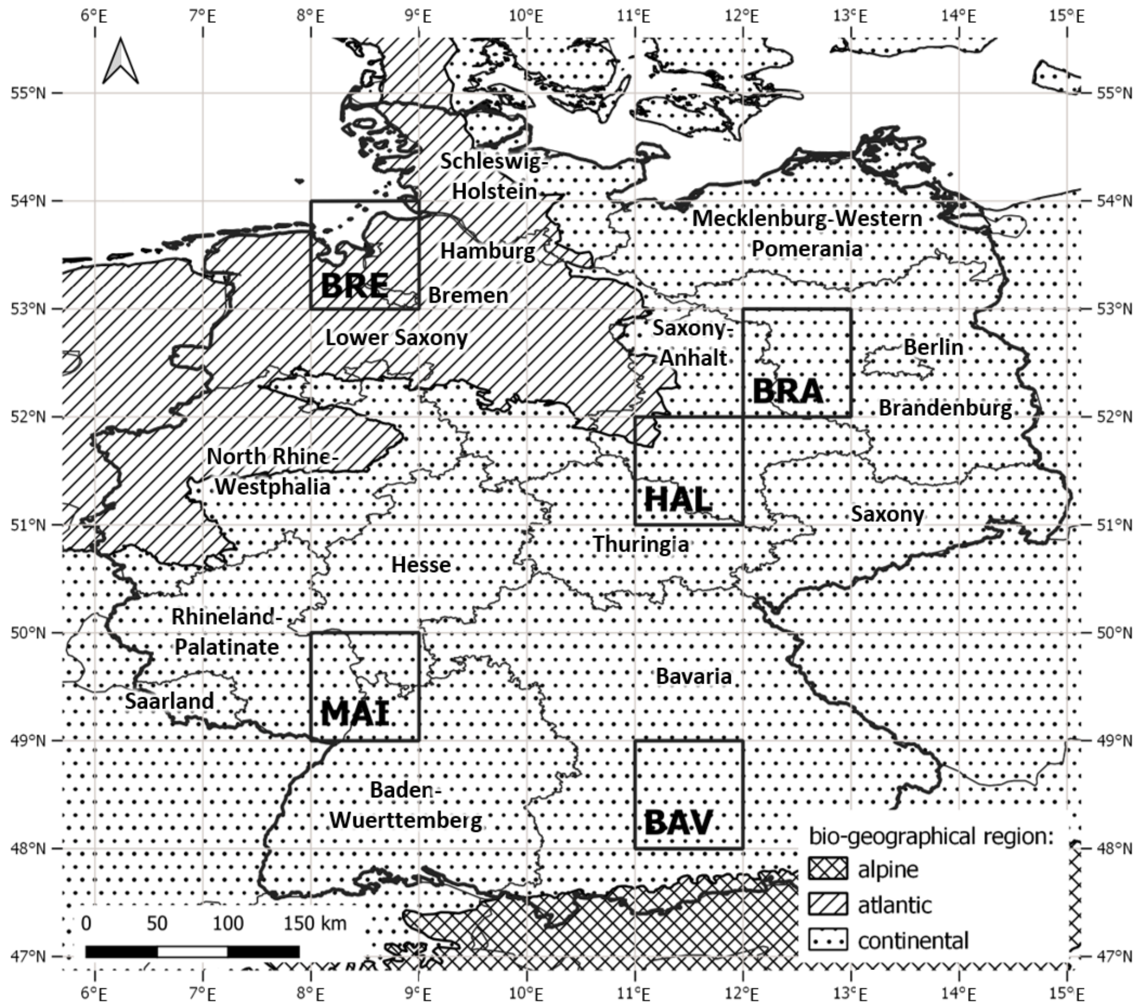

Figure 1: Coverage of the three bio-geographical regions in Germany and the location of the five test areas (BRE – Bremen, BRA – Brandenburg, HAL – Halle, MAI – Mainz, BAV – Bavaria).

3. Methods and Data

3.1 Using SCMaP for mapping soil exposure

SCMaP is used to build exposed soil masks containing all pixels in a given time period showing at least once exposed soil. For this purpose, a modified vegetation index (PV) (Rogge et al. 2018), based on the NDVI (Rouse et al. 1974), is used to separate the soils from other LC classes: PV = ((NIR - RED)/(NIR + RED)/((NIR - BLUE)/(NIR + BLUE)). Although authors have tested different indices for detecting bare soils such as BSI (e.g. Diek et al. 2017), combinations of NDVI + NBR2 (Demattè et al. 2018, Demattè et al. 2020), NBR2 and soil moisture indices (Vaudour et al. 2021) or NDVI and NDBI (Ying et al. 2017), we retain the PV index for this study in order to compare the results of the manual sampling with the automated sampling strategy. It is further important to remark that for the purpose of this study, the focus is not on selecting the purest soil pixels, but on creating an exposed soil mask that correspond to agricultural areas with changing covers and excludes all grasslands and deciduous forests.

To extract the exposed soil pixels, two composites containing the minimum (PV_{min}) and the maximum PV index (PV_{max}) per pixel are generated for a given time frame. Using the spatial and temporal behavior of the PV index values, two thresholds (T_{min} and T_{max}) are defined to distinguish the exposed soil areas from all other LC classes (Figure 2) to build the exposed soil mask. The determination of the thresholds is based on different LC classes (Figure 2a). Exposed soils (referred to as fields) and urban surfaces show the lowest PV values in the PV_{min} composite but also overlap with non-photosynthetic active vegetation (e.g., stubble on fields), dry grassland and deciduous forests. In the PV_{max} composite, soils are covered with vegetation, showing an overlap with forests and grasslands, and can be clearly separated from urban surfaces and areas showing permanent low vegetation indices, such as water. Therefore, the minimum threshold (T_{min}) is to separate urban surfaces and exposed soils from grassland, deciduous forests, coniferous forests and water. The maximum threshold (T_{max}) is set to distinguish the soils covered by vegetation from urban materials and water. By applying T_{min} and T_{max} thresholds to the PV_{min} and PV_{max} composites, two masks are generated. The intersection of the two masks results in the exposed soil mask.

As Rogge et al. (2018) demonstrated in detail, the lower 0.005 percentile of the deciduous forests defining T_{min} (Figure 2b) and the upper 0.995 percentile of the class urban are used to separate soils from all other LC classes (Figure 2c). These points are selected to avoid as many false positives as possible.

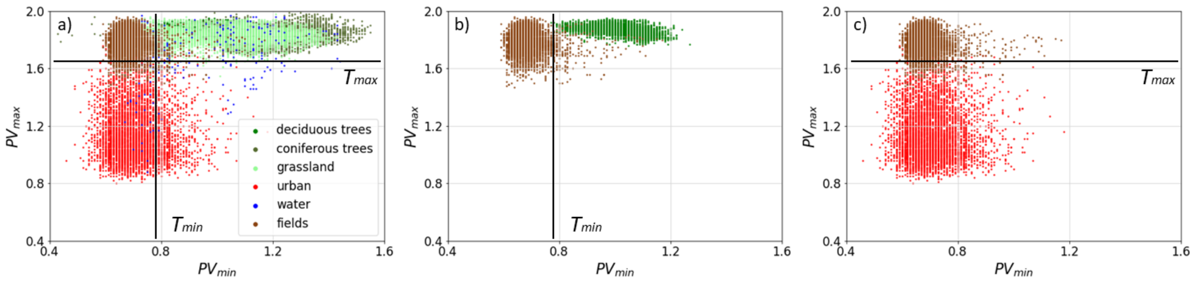

Figure 2: PV_{min} and PV_{max} characteristics of a) six LC types for the study area, b) the behavior of exposed soils (referred to as the LC class fields) and the LC class deciduous trees to define T_{min} and c) the behavior of fields and urban areas to define T_{max}.

3.2 Data preparation

3.2.1 Landsat data base preparation

The Landsat database used in this study is built from reprocessed Landsat-4 TM, Landsat ETM 5, Landsat-7 ETM+, and Landsat-8 OLI collection data sets provided by the USGS (Dwyer e al. 2018) for all path/row combinations covering Germany (Paths 192 to 197, Rows 22 to 27) between 1984 and 2019. The images were downloaded from the Google Archive in 2018 and 2019. All scenes available in the Level-1C processing state flagged with the highest correction level L1TP (calibration and orthorectification based on ground control points and digital elevation model data to correct for relief displacements (USGS 2020)) were downloaded. A total of 17,852 pre-processed Landsat images are used in this study (Table 1). SCMaP is applied to seven time periods from 1984 to 2019 each making use of five years of data. However, the first time period contains six years (1984-89).

Table 1: Overview of the number of pre-processed Landsat scenes available for all five-year time periods in the investigation area between 1984 and 2019.

time period	Landsat-4 TM	Landsat-5 ETM	Landsat-7 ETM+	Landsat-8 OLI	total
1984-89	85	1,772	-	-	**1,857**
1990-94	143	2,030	-	-	**2,173**
1995-99	-	1,986	211	-	**2,197**
2000-04	-	1,612	1,421	-	**3,033**
2005-09	-	1,946	1,154	-	**3,100**
2010-14	-	644	1,547	490	**2,191**
2015-19	-	-	1,319	1,982	**3,301**
1984-2019	**228**	**9,990**	**5,652**	**2,472**	**17,852**

For the seven composite periods, all available scenes per time period of the different sensors are combined. The merging of Landsat-4 TM, -5 ETM and -7 ETM+ images is a well-established method (Claverie et al. 2015, Kovalskyy and Roy 2015, Teillet et al. 2001). For the time period of 2015-19, scenes from Landsat-7 ETM+ and -8 OLI were combined, even though the equivalent bands for the calculation of the PV index of the two sensors contained slightly different wavelength ranges (Chastain et al. 2019). However, several studies have shown a minor to negligible influence resulting from merging the different wavelength ranges of Landsat-7 ETM+ and -8 OLI bands (Langford 2015, Xu and Guo 2014, Zhu et al. 2016, Roy et al. 2016, Holden and Woodcock 2016, Flood 2014). Based on these findings, the Landsat-7 ETM+ and Landsat-8 OLI data were merged as input to the SCMaP processing chain and were not separated for the generation of the 2015-19 composite.

For this study, Landsat collection data were used instead of the former Landsat pre-collection data, as the Landsat re-processed data sets provided a higher data quality (Li et al. 2019, Wulder et al. 2019) and showed fewer artifacts in direct comparison.

Several pre-processing steps were applied to the Landsat path/row scenes. The FMask algorithm (Zhu and Woodcock 2012, Zhu et al. 2015) detected and removed clouds, cloud shadows and pixels that were covered by snow. An atmospheric correction was applied to all scenes using Atmospheric Topographic Correction (ATCOR) software for satellite imagery (Richter and Schläpfer 2013, Richter 2010, Richter et al. 2006). Saturated pixels in urban areas and water bodies were identified and eliminated. Furthermore, manual filtering was performed to identify large-scale data artifacts as detector striping effects. The manually flagged path/row scenes (approximately 330 scenes) were excluded from the database. In particular, large artifacts covering a whole scene can substantially affect the SCMaP output, as the processor occasionally includes affected pixels in the exposed soil mask. Finally, the database was reorganized in 1° by 1° geographical tiles. For this purpose, lists of all intersecting path/row scenes per tile were generated and used by SCMaP for achieving efficient data handling and processing benefits.

3.2.2 Data preparation for automated sampling

Threshold determination requires the identification of known regions with no LC change over the observed time frame. For this purpose, temporarily stable LC areas without transition to other LC classes, preferably for the total investigation period (since 1984), are needed. The CORINE Land Cover (CLC) data set (EEA 2007) is a European data set containing repeated LC surveys that is provided by the EEA. To identify the stable areas, all available CLC layers and CLC change layers in vector format were downloaded (https://land.copernicus.eu/pan-european/corine-land-cover) and underwent several pre-processing steps (Figure 3b).

In a first step, the CLC classes that also contain land use components are reorganized and generalized to ensure that the resulting areas can be clearly assigned to a specific LC. The CLC data set consist of classes with different levels of detail. Figure 3a shows the summarized CLC subclasses for the subsequent threshold derivation (section 3.3). In addition, the CLC change layers containing the information regarding the transition of one LC class to another between two classification periods was subtracted from the data set. The reclassified and cleaned data sets were rasterized to the Landsat spatial resolution of 30 m. The removal of single pixels as well as a reduction of direct border pixels of individual class clusters was performed twice in order to exclude edge effects. To remove them, a three by three pixel moving window was used to analyze the relationships in a pixel neighborhood following von Neumann criteria (Toffoli and Margolus 1987). Finally, the resulting stable and cleaned data set contains LC pixels that did not change between 1990 and 2018 and are therefore called stable.

The threshold determination is built on randomly selected, automatically extracted stable CLC pixels based on different regional settings (Figure 3c), and is described in section 3.3.

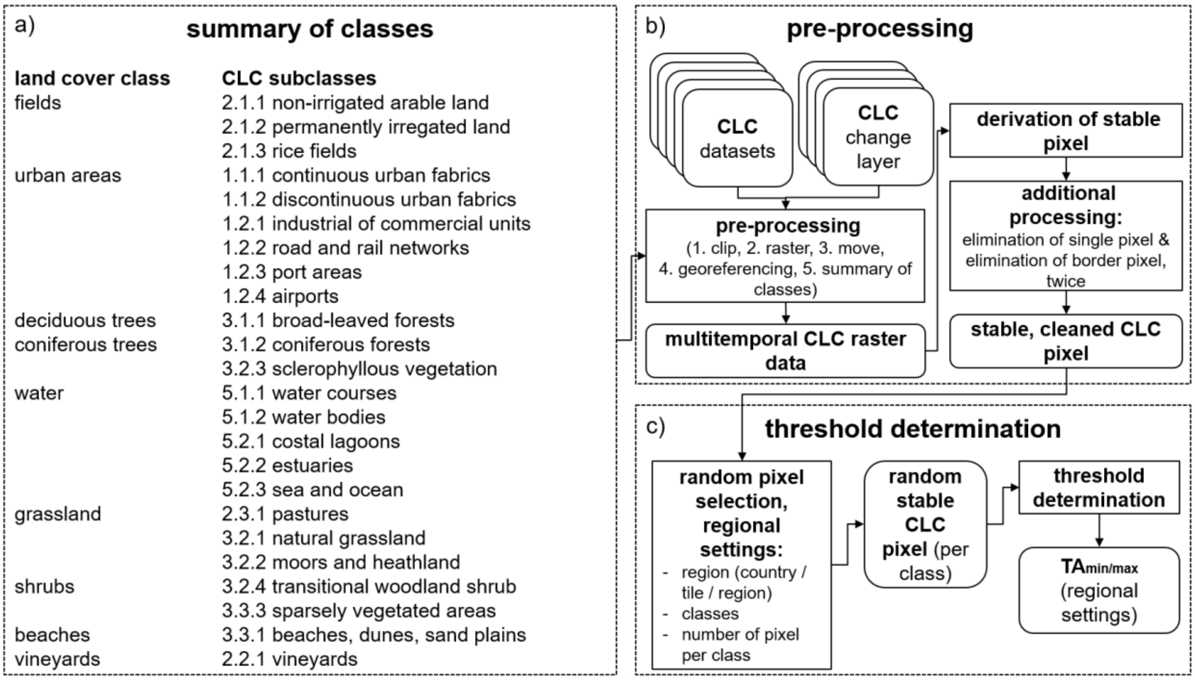

Figure 3: Workflow for the preparation of the LC data for the required threshold determination for SCMaP: a) summarized CLC classes used to build the nine LC classes for the automated selection of stable LC pixels; b) deviation of randomly selected stable CLC pixels; and c) subsequent threshold determination using regional settings per processing area (described in section 3.3).

3.2.3 Validation data sets

For the validation of the exposed soil masks for Germany generated by SCMaP, a country-wide data set is needed that can be assigned to exposed soils. Following the philosophy of SCMaP that is only extracting those exposed soil pixels that additionally show a change to vegetated condition in the observation time, a data set containing agricultural areas is needed.

For Germany, the statistical federal agency Destatis provides several surveys containing, for instance, the spatial size of agricultural areas in Germany per federal state and per county. These data sets are available for the years 1999, 2001, 2003, 2007, 2005, 2010 and 2016 (Destatis 2020 a, Destatis 2020 b). The general agricultural structure survey and agricultural census data sets were downloaded from the regional statistical database provided online by Destatis (https://www.regionalstatistik.de/genesis/online/logon). The surveys contain the number of farms and combined of agricultural area of common crop types, including grasslands in Germany per federal state and county. Because SCMaP is applied to an optical multispectral remote sensing database itis not possible to detect soils underneath permanent vegetation, the proportion of grasslands was excluded from the Destatis agriculture statistical analysis. All spatial information was converted to the percent coverage of agricultural area per federal state and per county using the size of each state and county provided by Destatis (Destatis 2018). As the SCMaP time periods of 2000-04 and 2005-09 contain two Destatis data sets each, the two respective statistics were averaged. For the states Berlin, Bremen, Hamburg and Mecklenburg Western Pomerania (Figure 1), no statistical data were available for any given time step. For the federal state of Saxony, data for a subset of the administrative districts were available.

The second validation data set used was the CLC inventories of 1990, 2000, 2006, 2012 and 2018 provided by the EEA (EEA 2007). The data sets were downloaded as vector files for Europe (https://land.copernicus.eu/pan-european/corine-land-cover), clipped to the extent of Germany, re-projected, resampled to the spatial resolution of the soil mask (30 m by 30 m) and saved as raster files. For validating the spatial distribution of the exposed soil masks in Germany extracted by SCMaP, the agricultural classes were of interest. The LC classes non-irrigated arable land (2.1.1) and permanently irrigated land (2.1.2) were extracted from the whole data set and summarized as the input for validation. For better comparability of the validation results to the Destatis survey, the percent coverage of the agricultural areas in the CLC data sets was also calculated per county and federal state.

3.3 Automated sampling and threshold derivation

Thresholds are necessary to separate exposed soils from all other LC classes. The objective is to derive thresholds that are applicable to the entire area of Germany. Therefore, a training data set that can be derived from the CLC mapping is needed, as described in 3.2.2. For this purpose, a new technique was developed that randomly selects CLC pixels that are stable over a long time period (section 3.2.2) and then applied to the Landsat database (section 3.2.1).

Originally, the threshold determination was based on the behavior of PV_{min} and PV_{max} of the manually selected LC pixels for the five test areas covering the spatial differences across Germany (see Rogge et al. 2018). The manual selection of LC pixels is a time-consuming step, which needs to be repeated for every processed region. Furthermore, the manual selection process can be influenced by the user. To overcome these limitations, an automated and random selection of LC pixels based on stable CLC pixels was developed. The stability of the new approach was tested via an in-depth comparison with the manual determination approach, and an analysis of the influence of the randomized selection procedure on the derivation of the thresholds was performed.

Due to the automated nature of the pixel selection procedure, several settings were tested to assess the performance of the new technique (Figure 3c). In this method, the area (tiles, countries, geographic regions, etc.), the LC classes (different amounts and composition of LC classes), the time steps, and the number of pixels per class can be selected individually, and enabling the assessment of the influence of these settings on the thresholds and the resulting exposed soil masks. To compare the random selection method with the manual selection method, the same regional settings were chosen. For this purpose, pixels were selected from the same five tiles covering Germany (Figure 1). A total of 5,000 stable CLC pixels per class and tile were selected using a random selection approach to avoid biased manual selection and a clustered distribution to ensure that all expressions of a land use class were recorded per region.

To determine the influence of the random selection approach on the thresholds, the temporal behavior of the LC classes needed to be analyzed in the first step. Therefore, the randomly selected $PV_{min/max}$ pixel values for the LC classes urban, deciduous trees and fields (presumably exposed soils), which are used to determine the thresholds, are shown in a histogram and compared to the $PV_{min/max}$ values derived from the manual selection approach.

Based on the $PV_{min/max}$ pixel values, the thresholds were defined. The defined thresholds based on manually selected LC pixels are referred to as $TM_{min/max}$ and were compared with the thresholds derived from the random selection approach ($TA_{min/max}$). In the first step, the applicability of the established percentiles for defining $TA_{min/max}$ was investigated. Furthermore, $TA_{min/max}$ were compared to the original sets of $TM_{min/max}$ for all tiles (2000-04; period with the largest overlap of data between Landsat-5 TM and -7 ETM+ and a minimum SCL failure of Landsat-7 ETM+) and all time steps of the Bavarian tile to investigate the spatial and temporal stability of the random selection approach. To estimate the influence of the random selection approach, ten sets of stable pixels per LC class (5,000 per LC class) for all tiles (2000-04) were selected. The influence of the $TA_{min/max}$ on the different sets of randomly selected pixels was investigated. Additionally, the absolute number of random stable pixels per class was altered. The influence of fewer (2,500) and more (10,000) stable pixels per class was investigated. Therefore, the $TA_{min/max}$ of ten sets of different numbers of randomly stable pixels per class for the Bavarian test tile (2000-04) were derived and compared.

3.4 Validation of the exposed soil masks in Germany

The processing of the SCMaP exposed soil masks (section 3.1) was performed by applying the averaged $TA_{min/max}$ of all five test areas (2000-04) (section 3.3) to all tiles in Germany for the seven time periods. The validation of the spatial and temporal distribution of the extracted exposed soil masks was performed using the two data sets described in section 3.2.3. The five prepared Destatis and CLC data sets were compared to the exposed soil masks for the time period containing the year in which each survey was conducted. To compare the validation data set and the mask, the coverage of the exposed soils extracted by SCMaP, expressed as percent, was calculated per federal state and county for each time step. To validate the spatial distribution of the exposed soil masks provided by SCMaP, a linear correlation analysis between the coverages of the exposed soil masks extracted by SCMaP and the agricultural areas provided by the Destatis statistics as well as the CLC data sets was explored for all 16 German federal states and at the county level. The comparison was evaluated by calculating the correlation coefficients (R^2) and root mean squared errors (RMSE) for each comparison to estimate the potential of SCMaP to build exposed soil masks for Germany based on the new thresholding method.

4. Results

4.1 Index thresholding

In Figure 4, the frequencies of the summarized $PV_{min/max}$ pixel values for the LC classes urban, fields and deciduous trees from all tiles comparing the manual and random pixel selection approaches are visualized, as these classes are relevant for the derivation of thresholds. For PV_{min}, the distributions are similar, excluding the LC class urban. Here, a clear shift of the maximum and a higher variability of PV_{min} values are visible. However, the shift of the class does not influence the determination of the TA_{min} as the LC class urban is not used to determine TA_{min}. Comparing the PV_{max}, the LC class shows a shifted and diversified distribution of values. The distribution of the LC classes deciduous trees and fields are less extreme and narrower than that of the manually selected pixels. Excluding the LC class urban, the $PV_{min/max}$ of the automated selected pixels shows a higher variance and standard deviation, whereas the median is similar. The shift and differing distribution of the PV_{max} of the LC class urban indicates an adaption of the point at which the TA_{max} has to be set to realize the separation between soils and other LC classes.

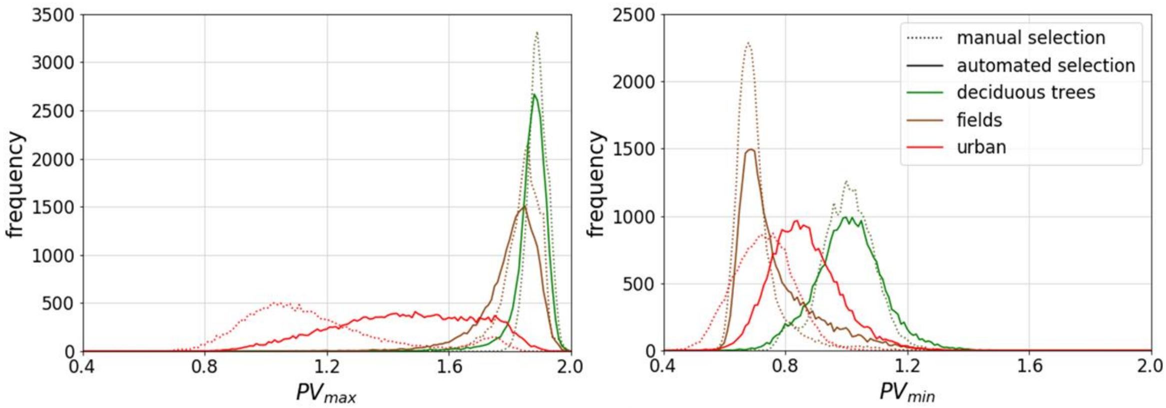

Figure 4: Histogram of the $PV_{min/max}$ frequencies summarized for all five test tiles comparing manual (dashed line) and random, automated (solid line) selected LC class pixels for the time step 2000-04.

The behavior of the LC classes urban and deciduous trees is used for the determination of $TA_{min/max}$ (Rogge et al. 2018). Comparing the scatterplots of the $PV_{min/max}$ values of the manually (Figure 5a) and randomly (Figure 5b) selected LC pixels, a lower clustering tendency of the data is visible. Mainly, the randomly selected pixel cluster of the LC class urban is not as selective compared to the manually selected pixel cluster. As mentioned, originally, the 0.995 percentile of the class urban was used to define the TM_{max}. Applying the 0.995 percentile to the automatically sampled pixels excludes almost half of the data cloud from fields and this, seems to be too high. Figure 5b shows that in the resulting exposed soil mask, a significant number of pixels is missing compared to the original exposed soil mask generated based on the manual sampling (Figure 5a). Therefore, an adjustment of the percentile to set the TA_{max} is required due to the less clustered distribution and the less selective behavior of the LC class urban (Figure 5b). For this purpose, a test has been designed by varying the TA_{max} from 0.995 to 0.89 for the exposed soil mask building.

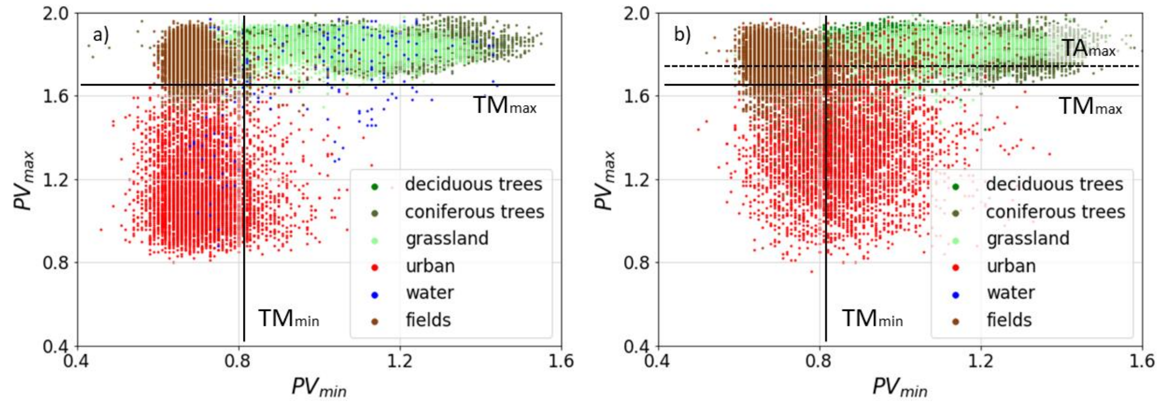

Figure 5: $PV_{min/max}$ pixel values for different LC classes comparing a) manual and b) randomly selected LC pixels and the derivation of TM_{max} and TA_{max} using the 0.995 percentile of the manually and randomly selected pixels of the LC class urban.

Figure 6 shows the result of this test for an area surrounding Aschersleben (within the test region HAL) in which different percentiles for the derivation of TA_{max} have been applied to the $PV_{min/max}$ composites (time period 2000-04). Based on CLC, approximately 78% of the land surface is covered by agricultural fields in the selected region. When using the TM_{max} value, 71% of the area is included in the exposed soil mask. Setting the TA_{max} at 0.995 results in a coverage of 36.6% in the same area. Using different TA_{max} values based on varying percentiles, the reduction in the percentiles used for setting the TA_{max} value resulted in an increase in the soil exposure mask saturating at the 0.94 percentile (TA_{max} = 1.723) (Figure 7*Figure **7***). As Figure 6 shows, a percentile of 0.90 for the LC class urban is used to define TA_{max}, and the resulting soil exposure is 71.3%, which is comparable to the soil exposure (71%) defined by TM_{max}.

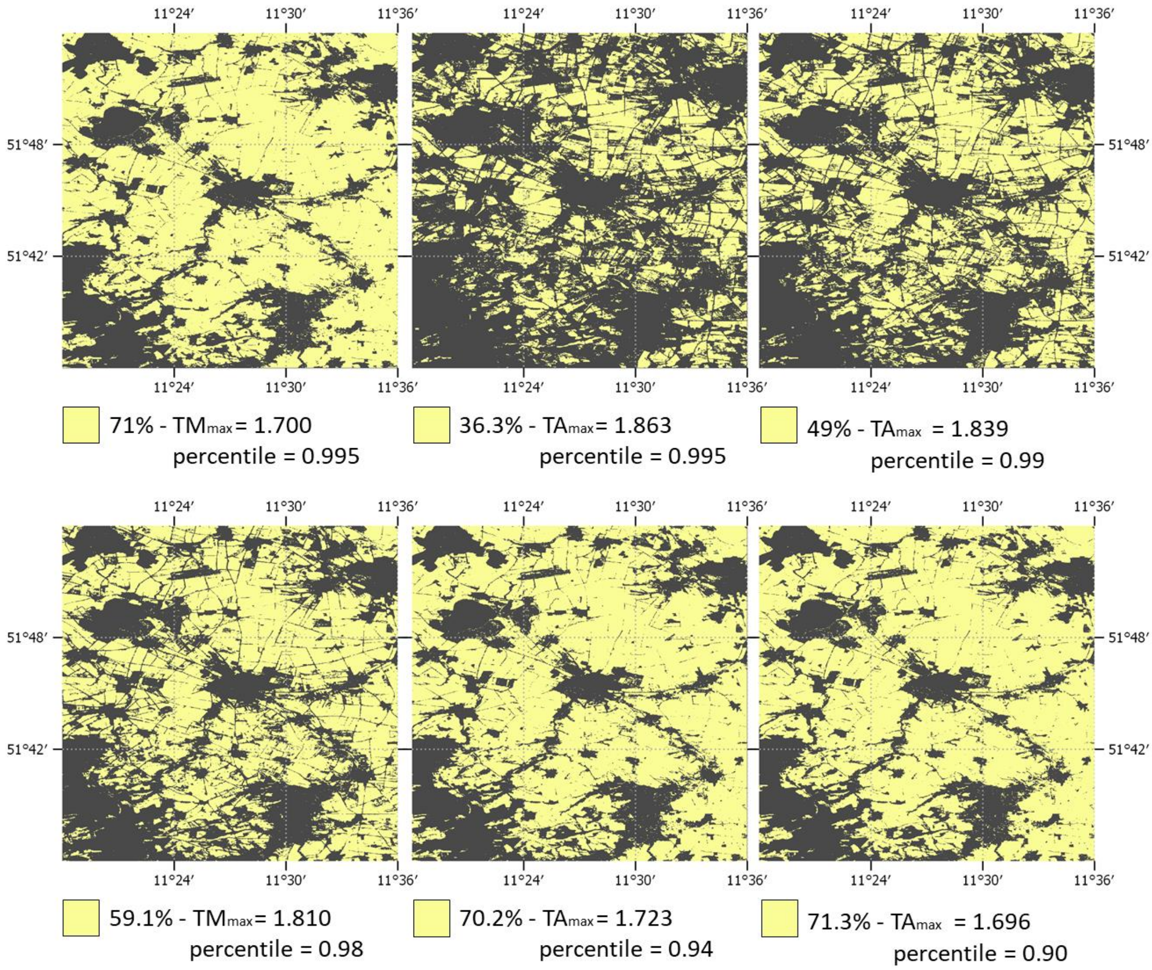

Figure 6: Influence of different percentiles on TA_{max} and the percentage coverage of the exposed soil mask in comparison to TM_{max} shown for the time period 2000-04 for an area near Aschersleben.

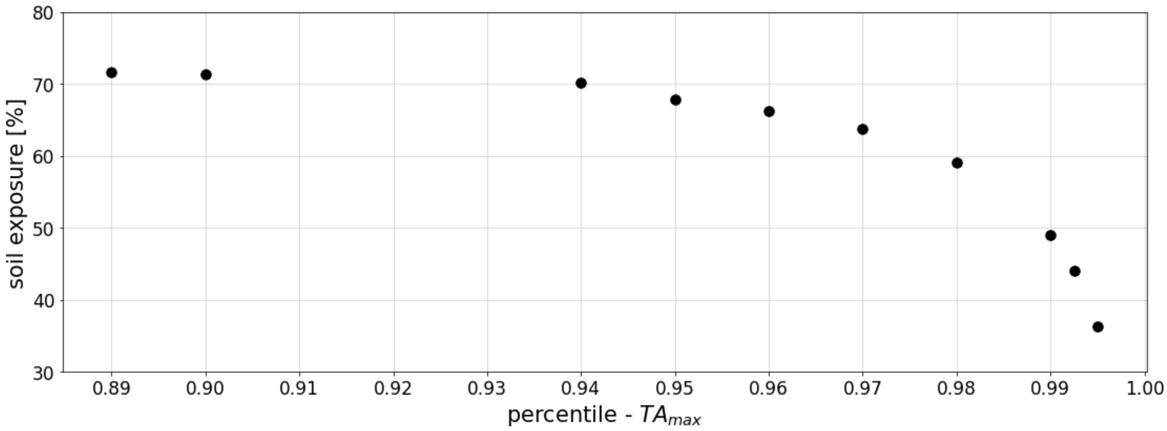

Figure 7: Varying soil exposure [%] determined for different percentiles to set the TA_{max} for an area around Aschersleben.

Following the selection of the percentile to be used in the definition of $TA_{min/max}$, Table 2 displays all $TA_{min/max}$ values and comparisons them to the $TM_{min/max}$ used across the different test areas for the time period of 2000-04 and for all time steps in the Bavarian tile. The $TA_{min/max}$ values for all areas are similar to the $TM_{min/max}$ values. Additionally, the averaged thresholds across the test areas fall within a similar range. The standard deviations across the test areas of $TA_{min/max}$ in comparison to $TM_{min/max}$ are slightly lower. For the different time steps of the Bavarian tile, the $TA_{min/max}$ values are also similar to the $TM_{min/max}$ values, reporting low standard deviations (STDs).

Table 2: $TA_{min/max}$ in comparison to $TM_{min/max}$ for all investigation areas (2000-04) and across time (only for Bavaria).

tile (time step)	**TM_{min}**	**TM_{max}**	**TA_{min}**	**TA_{max}**
BRE (2000-04)	0.896	1.831	0.866	1.795
MAI (2000-04)	0.803	1.675	0.823	1.635
HAL (2000-04)	0.836	1.762	0.844	1.666
BRA (2000-04)	0.861	1.467	0.827	1.701
BAV (2000-04)	0.758	1.749	0.744	1.685
average (areas – 2000-04)	**0.831**	**1.697**	**0.821**	**1.696**
STD (areas – 2000-04)	**0.053**	**0.140**	**0.046**	**0.060**
BAV (1984-89)	0.758	1.738	0.762	1.733
BAV (1990-94)	0.722	1.757	0.748	1.724
BAV (1995-99)	0.744	1.741	0.767	1.724
BAV (2005-09)	0.741	1.795	0.779	1.713
BAV (2010-14)	0.794	1.763	0.756	1.702
BAV (2015-19)	0.818	1.741	0.815	1.709
average (BAV – time)	**0.762**	**1.755**	**0.767**	**1.713**
STD (BAV – time)	**0.033**	**0.020**	**0.024**	**0.016**

Additionally, the reliability of the automated random selection of the stable LC pixels was investigated. The influence of the spatial distribution of the 5,000 randomly selected pixels was found to be minor though a comparison of ten sets of derived thresholds based on different sets of random stable pixels across the five test areas (Figures 8a and 8b). The ten sets of thresholds of each test area show few differences, which are evidenced by low standard deviations (0.002 to 0.005).

In addition to the spatial distribution of the random stable pixels, the influence of the total number of selected pixels on the determination of the thresholds was analyzed. Hence, ten sets of determined thresholds based on 5,000 randomly selected stable pixels per LC class were investigated and further compared to ten sets of 2,500 and 10,000 randomly selected stable pixels in the test area of Bavaria (Figures 8c and 8d). Overall, low standard deviations are observed (0.02 to 0.003), and the determined TA_{max} varies slightly (Figure 8c).

Due to the temporal and spatial stability of the defined thresholds and the statistically significant small influence of the location and number of random stable pixels, the presented derivation of the thresholds was found to be suitable for further processing steps.

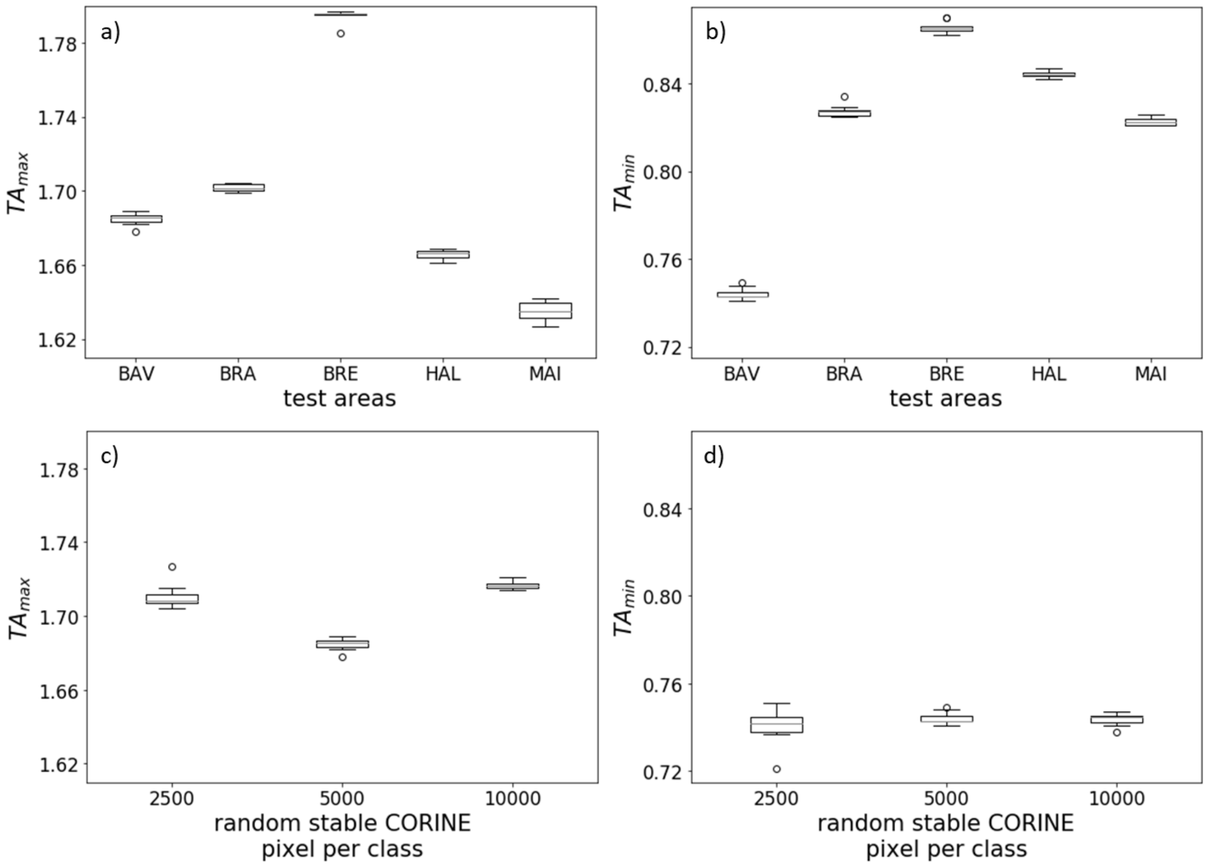

Figure 8: $TA_{min/max}$ variability across ten sets of randomly selected stable pixels for all test areas (2000-04) (a, b) and based on a different number of randomly selected stable pixels per LC class, extracted for the Bavarian tile (2000-04) (c, d).

4.2 Application of the new thresholds

The five sets of thresholds derived for the five test areas are averaged to one set of global thresholds, resulting in a TA_{min} of 0.831 and a TA_{max} of 1.697. Both thresholds were applied to all tiles in Germany to produce the exposed soil masks for all seven time periods.

These soil exposure masks contain pixels that show at least once exposed soil in the given time period. In addition, SCMaP provides two further binary masks per period containing the areas showing permanently low PV indices, which comprise urban areas, infrastructure, bare rocks and water bodies. In addition, a mask is generated in areas that show permanently high PV indices representing areas with permanent vegetation (e.g., grassland or coniferous trees). The combination of the three masks generates a generic LC classification of the investigation area (Figure 9).

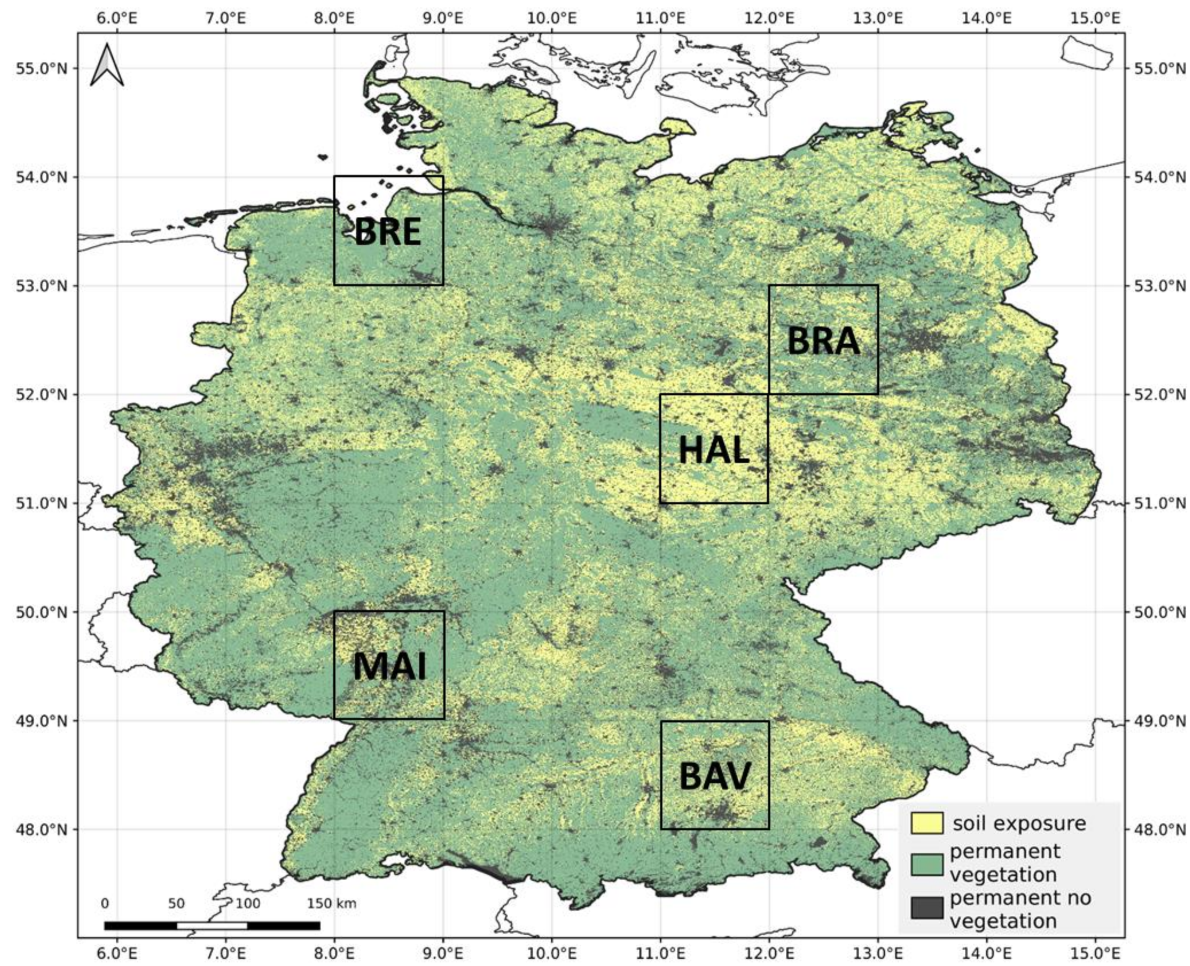

Figure 9: Generic LC classification for the study area showing pixels with soil exposure (yellow), permanent vegetation (green) and permanent no vegetation (gray) derived from 2000-04. The five test areas are marked.

Since the soil mask is available for several time steps between 1984 and 2019, changes in the spatial soil cover can be detected. Figure 10 (upper row) shows the temporal development of an area in western Munich (within the test region BAV). Here, areas with permanently low vegetation indices, which include the expansion of the city of Munich and the expansion of infrastructure, are increasing. Due to the expansion of Munich, a decrease in the area with exposed soils in the shown region is observed. Most agricultural areas have been transformed into settlement areas. The southern part is dominated by forests, where, in the early 1990s, a thunderstorm event deforested large portions, mainly in the southwest of Munich. The deforestation shows recovery in the subsequent time periods up until 2014. Here, the exposed soil areas gradually fill with permanent vegetation.

The bottom row of Figure 10 shows the development of two mining areas (Etzweiler and Garzweiler) near the city of Juelich in northeastern Germany. A spatial shift in the mining areas to different local regions can be seen. In addition to the spatial shift, a spatial expansion of the mining sites had resulted in a decreasing agricultural area around the sites.

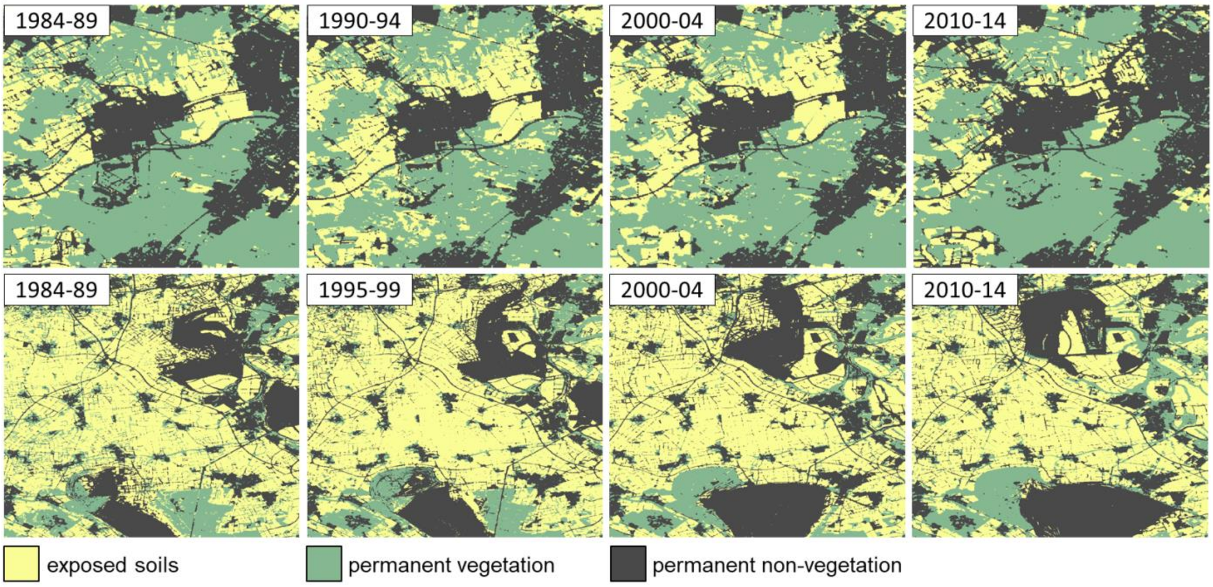

Figure 10: Detail of the generic land use classification showing the temporal development between 1984 and 2014 of a mainly urbanized area in the west of the city of Munich within BAV (upper row) and the temporal development of two mining areas (Etzweiler and Garzweiler) near Juelich (bottom row).

4.3 Validation of the exposed soil masks determined by SCMaP

The spatial and temporal distribution of exposed soil masks across Germany at several time steps is first validated according to Destatis statistics. The correlation coefficients (R^2) of the comparison for all 16 German federal states are shown in Table 3. Overall, high R^2 for all time steps and states can be derived. The lowest R^2 values are detected in the Lower Saxony state (0.59 to 0.78). Here, the agricultural area covers 37.95% of the total state. The highest R^2 values are reported in the states of Baden-Wuerttemberg (0.85 to 0.97), North Rhine-Westphalia (0.90 to 0.95) and Rhineland-Palatinate (0.90 to 0.94). For the states with a high amount of used agricultural area (Brandenburg, Saxony, Schleswig Holstein and Thuringia), the correlation coefficients are higher than 0.82 (Schleswig Holstein – SCMaP: 1995-99 / Destatis: 1999) per time step. As described above, the Destatis survey does not include all federal states as it does for the city states; no data are available for Mecklenburg-Western Pomerania and parts of Saxony.

Table 3: Correlation coefficients comparing the exposed soil masks determined by SCMaP to the agricultural areas provided by the statistical surveys by Destatis for all 16 federal states of Germany. However, some states were not included in the statistical survey due to missing data.

federal state	**agricultural area [%]**	**1995-99 / 1999**	**2000-04 / 2001/03**	**2005-09 / 20005/07**	**2010-14 / 2010**	**2015-19 / 2019**
Baden-Wuerttemberg	22.69	0.85	0.97	0.95	0.94	0.96
Bavaria	30.70	0.93	0.94	0.92	0.88	0.93
Berlin	8.58	-	-	-	-	-
Brandenburg	39.02	0.88	0.95	0.92	0.85	0.95
Bremen	8.62	-	-	-	-	-
Hamburg	6.61	-	-	-	-	-
Hesse	22.78	0.82	0.92	0.92	0.87	0.95
Mecklenburg-Western Pomerania	62.43	-	-	-	-	0.94
Lower Saxony	37.95	0.68	0.78	0.66	0.70	0.59
North Rhine-Westphalia	27.39	0.90	0.95	0.94	0.93	0.92
Rhineland-Palatinate	27.27	0.93	0.94	0.93	0.90	0.91
Saarland	14.30	0.80	0.91	0.86	0.82	0.94
Saxony	49.23	0.81	-	-	-	-
Saxony-Anhalt	60.26	0.84	0.88	0.92	0.91	0.94
Schleswig-Holstein	36.39	0.82	0.86	0.90	0.90	0.91
Thuringia	48.75	0.93	0.93	0.93	0.91	0.94

Additionally, the comparison between the exposed soil masks determined by SCMaP and the agricultural areas provided by CLC data sets show high R^2 values for each time step (Table 4). Comparing all federal states, the lowest correlation coefficients are reported for the state of Lower Saxony (0.61 to 0.86), as described for the validation with the Destatis data, whereas the highest correlation coefficients can be found for Baden-Wuerttemberg (0.91 to 0.97), Mecklenburg-Western Pomerania (0.91 to 0.97) and Rhineland-Palatinate (0.90 to 0.95). In contrast to the correlation of the exposed soil masks provided by SCMaP and the Destatis data, the state North Rhine Westphalia shows lower R^2 (0.84 to 0.92) comparing SCMaP and CLC. Overall, the states show similar R^2 when comparing to the correlation of the SCMaP and Destatis data. For the states with a large amount of agricultural area (i.e., the states of Brandenburg, Mecklenburg-Western Pomerania, Saxony, Schleswig Holstein and Thuringia), the correlation coefficients are higher than 0.80 (Schleswig Holstein – SCMaP: 1995-99 / Destatis: 1990) for all compared time steps. The high R^2 indicate high potential for the determination of exposed soil masks over time in agricultural areas.

Table 4: R^2 based on a comparison between the exposed soil masks derived by SCMaP and agricultural areas of the CLC data in comparison to the total amount of agricultural areas per state.

federal state	**agricultural area [%]**	**1990-94 / 1990**	**2000-04 / 2000**	**2005-09 / 2006**	**2010-14 / 2012**	**2015-19 / 2018**
Baden-Wuerttemberg	22.69	0.91	0.92	0.91	0.94	0.97
Bavaria	30.70	0.85	0.90	0.86	0.90	0.84
Berlin	8.58	-	-	-	-	-
Brandenburg	39.02	0.80	0.92	0.94	0.91	0.97
Bremen	8.62	-	-	-	-	-
Hamburg	6.61	-	-	-	-	-
Hesse	22.78	0.82	0.95	0.93	0.92	0.97
Mecklenburg-Western Pomerania	62.43	0.91	0.96	0.94	0.92	0.99
Lower Saxony	37.95	0.68	0.86	0.79	0.75	0.61
North Rhine-Westphalia	27.39	0.84	0.92	0.91	0.91	0.90
Rhineland-Palatinate	27.27	0.90	0.95	0.92	0.94	0.93
Saarland	14.30	0.85	0.88	0.90	0.95	0.99
Saxony	49.23	0.90	0.95	0.96	0.93	0.84
Saxony-Anhalt	60.26	0.86	0.95	0.96	0.97	0.95
Schleswig-Holstein	36.39	0.90	0.65	0.94	0.92	0.80
Thuringia	48.75	0.91	0.96	0.96	0.96	0.94

In addition to the correlation per federal state, a comparison at the county level was conducted. High R^2 values and low RMSE values (Figure 11) demonstrate that SCMaP captures the exposed soil masks in Germany well. For all time periods, high correlations between the percentage proportion of SCMaP exposed soil masks and the agricultural areas provided by statistical surveys of Destatis are identified. The highest correlation can be found for the SCMaP time period 2000-04 ($R^2 = 0.88$) compared to the respective averaged Destatis data sets of 2001/03, whereas the SCMaP time period 1995-99 shows the lowest correlation ($R^2 = 0.82$) compared to the corresponding Destatis data set from 1999. Although the general correlation is high, there is a minor systematic underestimation of the higher soil exposure values in all analyzed time periods (Figure 11).

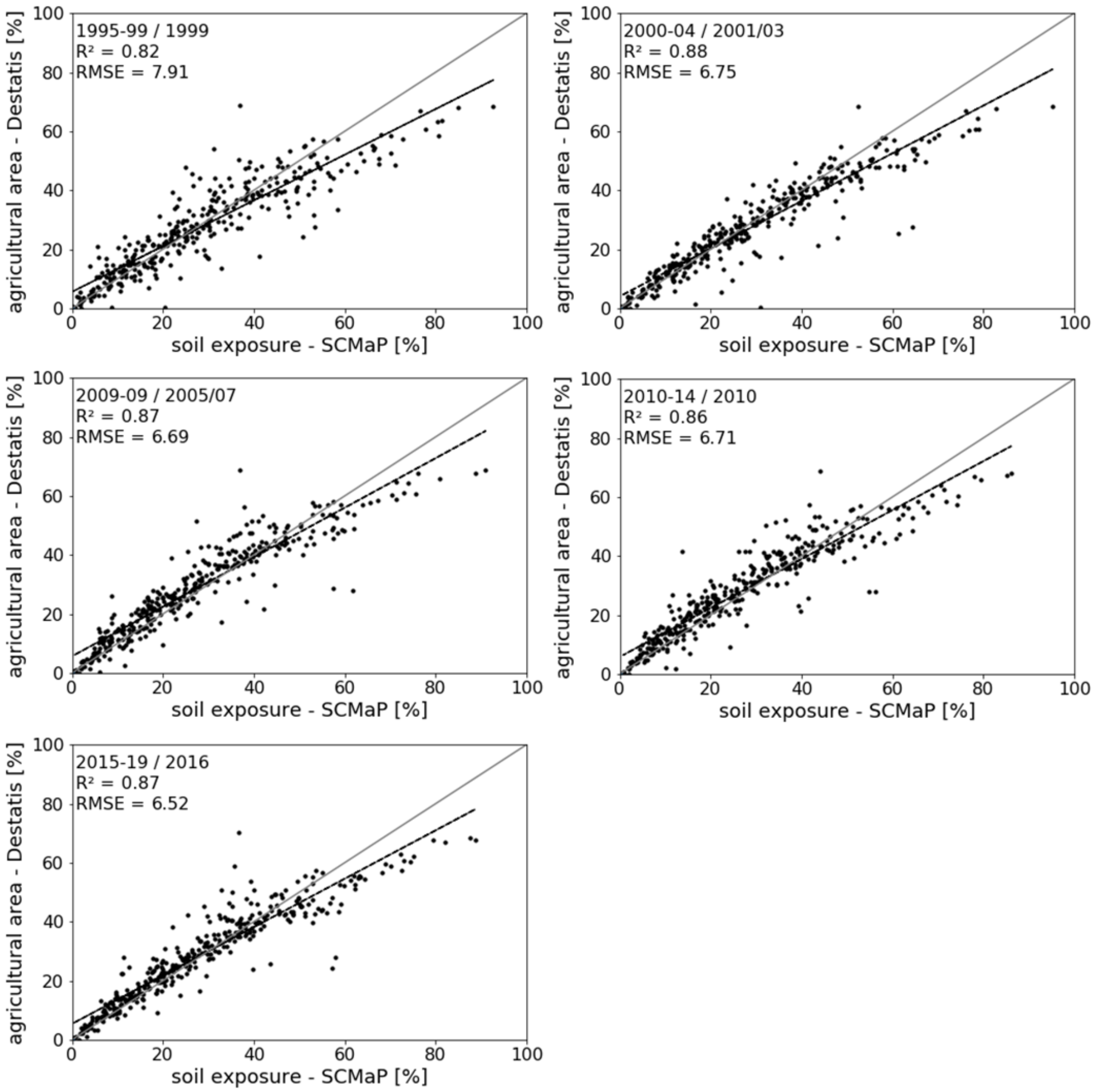

Figure 11: Regression between exposed soil masks identified by SCMaP and the agricultural areas based on Destatis at the county level for Germany.

Moreover, a linear correlation analysis comparing the percentage of exposed soil masks per county derived by SCMaP to the percentage of agricultural areas provided by the CLC data sets was performed. The results show a strong correlation between the tested data sets (Figure 12). The highest correlation is reported for the SCMaP periods of 2000-04 and 2005-09 to the CLC data sets of 2000 (R^2 = 0.89) and 2006 (R^2 = 0.88), respectively. The weakest correlation can be found for the SCMaP time period of 1990-94 when compared with the CLC data set from 1990 (R^2 = 0.80). Overall, low RMSE values are observed.

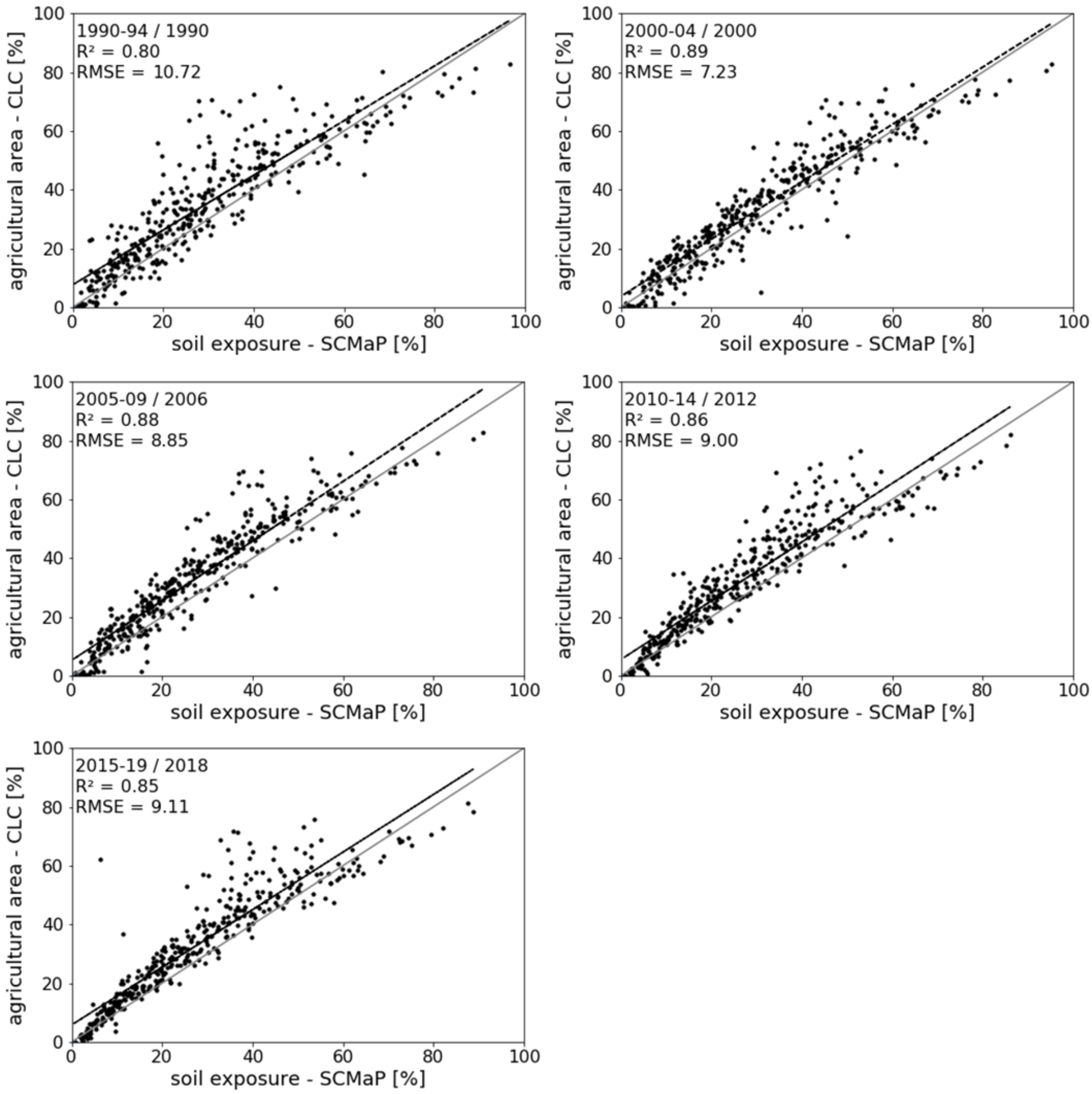

Figure 12: Regression between exposed soil masks extracted by SCMaP and the agricultural used areas based on CLC data for all counties in Germany.

Figure 13 shows the variability between the differences in the percentages of exposed soil masks extracted by SCMaP and the portion of agricultural areas provided by the validation data sets for all counties and compared time steps. Comparing the exposed soil masks extracted by SCMaP to the agricultural areas based on the Destatis surveys, a deviation to the mean, ranging on average between -1.46% (SCMaP: 2005-09 / Destatis: 2007) and +1.43% (SCMaP: 2000-04 / Destatis: 2001/03), is detected. However, the range of 50% of the counties varies between ±5.04% (SCMaP: 2005-09 / Destatis: 2007) and ±7.38% (SCMaP: 1995-99 / Destatis: 1999). Excluding the outliers, there is a small absolute difference between the percentage of agricultural areas documented by the Destatis surveys and the exposed soil masks derived by SCMaP. The differences between the percentages of exposed soil masks extracted by SCMaP and the CLC-derived agricultural areas show a slightly stronger underestimation, ranging between -5.61% (SCMaP: 2005 / CLC: 2006) and -2.90% (SCMaP: 2000-04 / CLC: 2000). Excluding the outliers, the range of 50% of the counties varies between ±5.63% (SCMaP: 2005-09 / CLC: 2006) and ±3.42% (2000-04 / CLC: 2000).

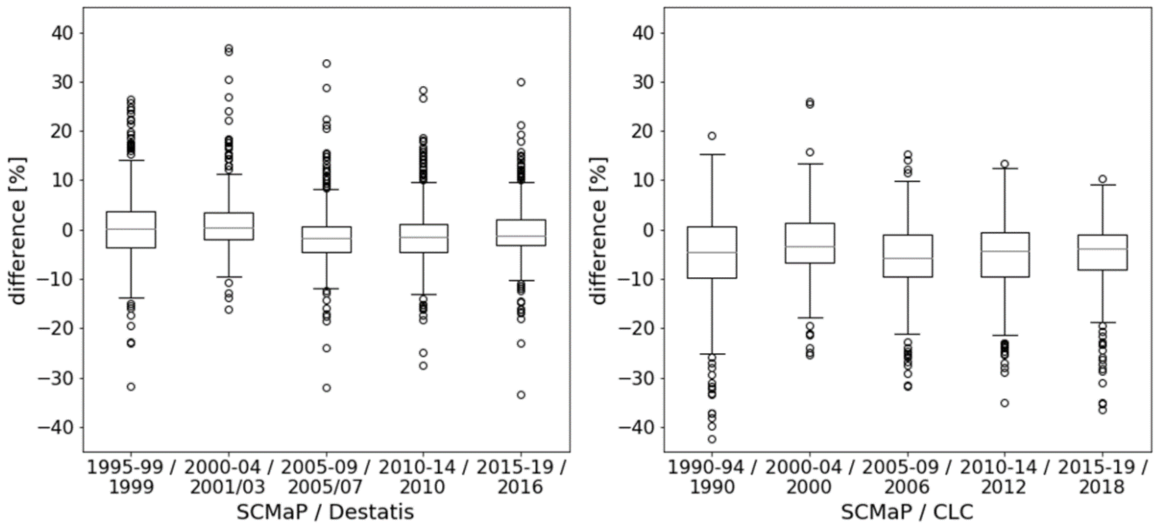

Figure 13: Variability of the differences in exposed soil masks extracted by SCMaP compared to the validation data sets of Destatis and CLC based on all counties in Germany for all time periods.

Overall, the comparison between both validation data sets indicates a high consistency across all time periods. In particular, the time periods of 2000-04 and 2005-09 show the highest correlation coefficients and lowest RMS errors for both validation data sets compared at the state (Tables 3 and 4) and county level (Figures 11 and 12).

5. Discussion

5.1 Sampling and threshold definition

Section 4.1 shows the results of the different settings used to derive the $TA_{min/max}$ thresholds. The random selection of stable CLC pixels demonstrates an overall minor influence on the frequency distribution of LC classes, such as deciduous trees and fields, comparing the $PV_{min/max}$ behaviors in relation to the manually selected LC pixels. The main differences were found for the class urban (Figures 4 and 5). The manual selection of the land cover class urban was concentrated in the downtown areas of metropolitan regions (e.g., central Munich in the Bavarian test tile), the random selection of stable CLC pixels resulted in an even distribution across the complete tile. This better captures the variability associated with urban structures (e.g., densely to less densely populated areas, industry, infrastructure, etc.) and can also include vegetated pixels from parks or trees and lawns along streets. The less clustered selection influences the frequency distribution of the PV indices for the land cover class urban and thus, more pixels have higher PV_{max} values (Figure 4).

To account for the differences in the distribution of the LC classes in the PV_{max} composite, an adaptation of the percentile used for the determination of the TA_{max} was necessary. Figure 6 and 7 show the influence of the modified percentile rule depending on the spatial-temporal behavior of the analyzed LC. However, we observed a gradual decrease ($TA_{max} = 0.89 – 0.98$) followed by a rapid decrease ($TA_{max} > 0.99$) of the resulting soil exposure. A decrease of the percentile (0.995 to 0.900) for the definition of the TA_{max} enabled the generation of an exposed soil mask (Figure 6) comparable to the coverage of agricultural area provided by the reference data set and comparable to the soil exposure mask based on the manual derived TM_{max} for an example area in the Halle test tile.

The adapted percentiles were the basis for further analyses. In this way, thresholds have been derived separately for the five different regions across Germany (Figure 8). In particular, the TA_{max} of Bremen is higher than the four other TA_{max} values (Figure 8a). Although the $TA_{min/max}$ values of the individual test sites are comparable to the averaged $TM_{min/max}$ of all five areas, the derivation of exposed soil masks could be affected, especially for the region near Bremen. A varying $TA_{min/max}$ value may impact the classification of exposed soil masks, so it might be more feasible to process all of Germany not only using one set of $TA_{min/max}$. A scheme summarizing comparable areas should be established. This could include replacing political borders with larger geographically homogenous units. For this purpose, the biogeographical regions (section 2 and Figure 1) (EEA 2016) could provide a valuable baseline for the definition of the thresholds. Germany is covered mainly by the continental biogeographical region (the test areas Bavaria, Mainz, Brandenburg and Halle), whereas the areas near Bremen, as the northwestern part of Germany, are covered by the atlantic bio-geographical region. Applying SCMaP with $TA_{min/max}$ adapted to the different regions could reduce the local effects on the thresholds and improve the extraction of exposed soil masks.

Finally, we tested the influence of the number of pixels per class selected for the threshold determination and found almost no influence. This suggests that regardless of the number of selected pixels, the thresholds are very stable when they are equally distributed over the area of interest.

In summary, the new automated sampling is a very flexible and robust method to provide the data base for the threshold derivation, whereas the threshold definition based on percentile seemed not as the best method although its simplicity (Lobell et al. 2007, Zhao et al. 2012, Avisse et al. 2017, Thonfeld et al. 2020, Zhuo et al. 2019). In this study, an adaption of the percentile rule was necessary for the changed sample data set and it is very likely that the percentile rule need to be changed again if a different area is explored. Therefore, in the future, alternative methods to extract exposed soil pixels should be tested for instance regression and classification methods such as logistic regression (Kleinbaum et al. 2002), Random Forests (Breiman 2001) or maximum likelihood classification (Richards 1993) or any other machine learning approaches. For this study, it was important to use the same methodology as for the manual sampling to obtain the highest possible comparability to the method of Rogge et al. (2018).

5.2 Validation of the exposed soil masks across Germany

We have chosen TA_{min} of 0.831 and TA_{max} of 1.697 as the best results and used them for the generation of exposed soil masks for several time periods. We validated the extraction of exposed soil masks per selected time periods at the federal state and county level by using the Destatis and CLC data sets (see section 4.3). The comparison of the soil exposure with both validation datasets showed overall high correlation results ($R^2 > 0.80$ on county level for) for all time periods (Tables 3 and 4, Figures 11 and 12).

In particular the five-year periods of 2000-04 ($R^2 = 0.88$ for Destatis; $R^2 = 0.89$ for CLC) and 2005-09 ($R^2 = 0.87$ for Destatis; $R^2 = 0.88$ for CLC) show the overall highest R^2, and the periods of 1990-94 ($R^2 = 0.80$ for for CLC) and 1995-99 ($R^2 = 0.82$ for Destatis) show the weakest R^2

comparing the exposed soil masks to the agricultural areas of the validation datasets on county level. These results are similar at the state levels based on both validation datasets. The high R^2 in the periods of 2000-04 and 2005-09 might correlate to the high availability of input data. In 2000-04 and 2005-09; even though the scan line correction failure of Landsat-7 ETM+ appeared in 2002 (Markham et al. 2004), over 3,000 pre-processed input images were available (2000-04: 1946 Landsat-5 TM, 1154 Landsat-7 ETM+; 2005-04: 1946 Landsat-5 TM, 1154 Landsat-7 ETM+). In comparison to the 1990-94 and 1995-99 periods with lower R^2 values, less than 3,000 images per composite were available (1990-94: 1857, 1995-99: 2681 pre-processed scenes). This availability of scenes resulted in a large number of cloudless scenes per pixel (Table 5). On average, 56.0 ± 18.6 (2000-04) and 59.0 ± 17.6 (2005-09) cloudless scenes per pixel were included in the database for the extraction of exposed soil masks for Germany. In contrast, there were 44.3 ± 15.0 and 41.7 ± 14.2 cloudless scenes that built the database for the time periods of 1990-94 and 1995-99, respectively. For the time periods showing weaker R^2 values, fewer cloudless input scenes are available per pixel, which could indicate a higher deviation from the validation data. Here, too few data are available to capture the exposed soil masks with high accuracy compared to the following periods.

Table 5: Average cloudless scenes per pixel for Germany and R^2 at the county level per time period.

time period	average cloudless scenes per pixel (Germany)	STD (Germany)	maximum cloudless scenes per pixel (Germany)	R^2 (SCMaP – Destatis)	R^2 (SCMaP – CLC)
1984-89	35.0	12.1	112	-	-
1990-94	44.3	15.0	112	-	0.80
1995-99	41.7	14.2	134	0.82	-
2000-04	56.0	18.6	102	0.88	0.89
2005-09	59.0	17.6	140	0.87	0.88
2010-14	41.6	12.3	104	0.86	0.86
2015-19	49.7	19.4	146	0.87	0.85

The correlation analysis showed an overall high R^2 for Germany on the state and county levels (Tables 3 and 4, *Figure **11***Figures 11 and 12). The federal state of Lower Saxony shows a lower R^2 for all time periods for both scenarios compared. An in-depth review of the input data has shown no data artifacts or comparable data quality limitations for the federal state or the entire region in northwestern Germany. A possible source of the low accuracy of the soil mask in Lower Saxony could be the lower number of cloudless scenes per pixel in comparison to all of Germany. The number of maximum cloudless scenes per pixel for the Lower Saxony state is lower than the cloudless scenes available for all of Germany (section 5.1). In Germany, a maximum number of 102 (2000-04) to 140 (2005-09) are available for the extraction of exposed soil masks. For the state of Lower Saxony, a maximum number of 70 (1984-89) to 110 (1995-99) cloudless scenes are available. This difference could have been driving the deviation in accuracy, as a certain number of scenes should be available for the extraction of exposed soils.

Furthermore, as described in section 4.2, all of Germany was processed using the averaged $TA_{min/max}$ of the five test tiles. However, as discussed above, the $TA_{min/max}$ value of Bremen, situated in the center of Lower Saxony, varies more relative to the other four sets of TAs. Considering that the different thresholds have an influence on the extraction of the soil pixels, the use of the bio-geographical region as the definition of thresholds in Germany could result in better adjustment to the natural conditions present in the northwestern parts of the country.

However, it should be mentioned that a possible source of inaccuracy could have resulted from the comparison of a multiyear composite with a validation data set collected in one year. In all five-year composites, areas that show at least one exposed soil in the observed time period are included in the exposed soil mask. The selection of the longer time period was performed based on previous experience as it guaranteed the capture of all agricultural exposed soils. As the five-year periods are compared to one reference data set, changes in land use could have had an influence on the accuracy analysis. For instance, if a transition of permanent grassland to exposed soils occurred early within an observed period, the possibility of obtaining a sufficient number of available scenes showing exposed soils is high. SCMaP would then classify these areas correctly as exposed soils. For validation purposes, a comparison to a data set recorded early in the five-year period would then result in an erroneous identification of the area by SCMaP. As the five-year composites contain two LC types; grassland and exposed soils; however, the classification by SCMaP for exposed soils is correct. A reduction in the time for compositing could enable a decrease in the occurrence of such cases.

For validation purpose of the SCMaP exposed soil masks two different data sets were chosen. The Federal Statistical Office (Destatis) collects statistical data regarding agricultural areas in Germany on a regular basis since 1999. However, determining the methods used for the data collection is in the responsibility of each federal state and might result in regional differences. Additionally, the lowest available spatial resolution is on county level. For that purpose and for future continental processing, we additionally used the agricultural classes of the CLC surveys for the validation of exposed soil masks as the data sets are available since 1990. Although the CLC inventories are derived from a pixel-based classification, the data also shows a lower spatial resolution than the SCMaP exposed soil masks. This demonstrates that both data sets have their advantages and disadvantages for the validation of the exposed soil masks, since both comparisons showed systematic differences with respect to lower correlations of the earlier periods and regarding to lower R^2 for the federal state Lower Saxony. However, since both validation results are similar and in the same order of magnitude, we believe that they represent realistic accuracy values. Both datasets seem to be suitable for large scale accuracy analyses, whereas CLC has the potential for a European-wide validation of the detection of exposed soils.

6. Conclusion and Outlook

In this study, we analyzed the influence of the new automated sampling strategy on thresholding and the derivation of exposed soil masks. Further, we provided a Germany-wide validation for several time periods in order to show the accuracy of the resulting exposed soil masks across time. An automatized random sampling of stable CLC pixels required for the determination of two thresholds ($TA_{min/max}$) to separate exposed soils from all other LC classes was developed and implemented in the SCMaP processing chain. The automatization of the thresholding process is necessary for operational processors to ensure the fast and correct adaption of the thresholds to regions of interest and to provide regionalize thresholds for the processing of large areas, such as countries and continents. Our results demonstrated the large dependencies that the vegetation index approach has on environmental conditions. Thus, we suggest regionalizing the parameter setting by using e.g., bio-geographical regions instead of counties or countries. Furthermore, the rules to derive thresholds need to be evaluated depending on the sample database. In this study, we used CLC information;

however, we would not suggest applying a fixed percentile rule since it needs to be adapted according to the sampling scheme. A more robust method that accounts for the minimal overlap of spectral similar LC classes would be more suitable. Additionally, the nature of fixed thresholds for large regions are not suggested. A flexible method to derive region-specific thresholds or the use of dynamic thresholds using machine learning techniques or artificial intelligence approaches could be a valuable topic for future developments. The implementation of such approaches in operational processors is important for future studies. For this purpose, the automated and robust sampling such as developed in this study is of high importance.

The validation using two independent reference data sets again shows the need to account for the regional differentiation of the thresholds. For both data sets (CLC and Destatis) we selected agricultural classes that can be assigned to exposed soils. Areas in northwestern Germany have shown a systematic underestimation of exposed soils compared to both reference data. Additionally, there is a difference in R^2 based on the number of available input scenes per time step. We could show that the more scenes per time period are available, the higher the percentage of cloudless scenes and thus, the higher the R^2. The implementation of Sentinel-2 data could potentially shorten the recent composite time length of five years. This is also in line with the findings of Demattè et al. (2018). Sentinel-2 delivers data from two twin satellites with a combined revisit time of less than five days (Lacroix et al. 2018, Ienco et al. 2019). The use of Sentinel-2 data could therefore result in the increased accuracy in the building of exposed soil masks and the shortening of the compositing time period. Additionally, the current developed “Harmonized Landsat and Sentinel-2 surface reflectance data set” (Claverie et al. 2018) should be considered. Since both data sets have been pre-processed following the same protocols and methods, this data set could be a highly valuable input regarding the large number of available scenes and needs to be analyzed in the future. This could enable monitoring of soil properties more frequently than every five years.

In summary, the automated and random sampling of LC pixels for the determination of thresholds is a stable and reliable workflow that enables the identification of the spatial and temporal distribution of exposed soils with high accuracy. Thus, it can be a valuable data source for statistical surveys of agricultural areas in Germany. SCMaP is additionally used to generate information about how frequently soils are exposed and how often these areas shift from exposure to vegetation. To contribute to soil erosion studies that need information about where and when soils are bare, accurate exposed soil masks in suitable time period can be of great help for these studies (Pimentel and Burgess 2013, Labriere et al. 2015, Ayalew et al. 2020). The exposed soil masks derived from SCMaP can additionally offer a new remote sensing database for retrospective erosion and LC analysis.

Literature

Adams, B., Iverson, L., Matthews, S., Peters, M., Prasadm, A., Hix, D.M., 2020. Mapping Forest Composition with Landsat Time Series: An Evaluation of Seasonal Composites and Harmonic Regression. Remote Sensing, 12, 610.

Adhikari, K., Hartemink, A.E., (2016): Linking soils to ecosystem services – A global review. Geoderma, 262 (2016), 101-111.

Avisse, N., Tilmant, A., Müller, M.F., Zhang, H., 2017. Monitoring small reservoirs' storage with satellite remote sensing in inaccessible areas. Hydrol. Earth Syst. Sci, 21, 644-6459.

Ayalew, D.A., Deumilch, D., Sarapatka, B., Doktor, D. 2020. Quantifying the Sensitivity of NDVI-Based C Factor Estimation and Potential Soil Erosion Prediction using Spaceborne Earth Observation Data. Remote Sensing, 12, 113.

Baude, M., Meyer, B.C., Schindewolf, M., 2019. Land use change in an agricultural landscape causing degradation of soil-based ecosystem services. Science of the Total Environment, 659, 1526-1536.

Borelli, P., Panagos, P., Montanarella, L., 2015. New insights into the Geography and Modelling wind Erosion in the European Agricultural Land. Application of a Spatially Explicit Indicator of Land Susceptibility to Wind Erosion. In: Sustainability, 7, 8823-8836

Borelli, P., Lugato, E., Montanarella, L., Panagos, P., 2017. A new assessment of soil loss due to wind erosion in European agricultural soils using a quantitative spatially distributed modelling approach. In: Land Degradation & Development, 28, 335-344; DOI: 10.1002/ldr.2588.

Borelli, P., van Oost, K., Meusburger, K., Alewell, C., Lugato, E., Panagos, P., 2018. A step towards a historic assessment of soil degradation in Europe: Coupling on-site erosion with sediment transfer and carbon fluxes. In: Environmental Research, 161, 291-298; DOI: 10.1016/j.envres.2017.11.009.

Breiman, L., 2001. Random Forests. Machine Learning, 45, 5–32

Cerdan, O., Govers, G., Le Bissonnaus, X., van Oost, K., Poesen, J., Saby, N., Gobin, A., Vacca, A., Quinton, J., Auerswald, K., Klik, A., Kwaad, F.J.P.M., Raclot, D., Ionita, I., Rejman, J., Rousseva, S., Muxart, T., Roxo, M.J., Dostal, T., 2010. Rates and spatial variations of soil erosion in Europe: A study based on erosion plot area. In: Geomorphology, 12, 167-177.

Chastain, R., Housman, I., Goldstein, J., Finco, M., Renneson, K., 2019. Empirical cross sensor comparison of Sentinel-2A and 2B MSI, Landsat-8 OLI and Landsat-7 ETM + top of atmosphere spectral characteristics over the conterminous United States. Remote Sensing of Environment, 221, 274-285.

Claverie, M., Vermote, E.F., Franch, B., Masek, J.G., 2015. Evaluation of the Landsat-5 TM and Landsat-7 ETM + surface reflectance products. Remote Sensing of Environment, 169, 390-403.

Claverie, M., Ju, J., Maesk, J.G., Dungan, J.L., Vermote, E.F., Roger, J.-C., Skakun, S.V., Justice C., 2018. The Harmonized Landsat and Sentinel-2 surface reflectance data set. Remote Sensing of Environment, 219, 145-161.

Daughtry, C.S.T., Doraiswamy, P.C., Hunt Jr., E.R., Stern, A.J., McMurtrey III, J.E., Prueger, J.H., 2006. Remote Sensing of Crop Residue Cover and Soil Tillage Intensity. Soil and Tillage Research, 91, 1-2, 101-108.

Demattè, J.A.M., Fongaro, C.T., Rizzo, R., Safanelli, J.L., 2018. Geospatial Soil Sensing System (GEOS3): A powerful data mining procedure to retrieve soil spectral reflectance from satellite images. Remote Sensing of Environment, 212 (2018) 161-175.

Demattè, J.A., Safanelli, J.L., Poppiel, R.R., Rizzo, R., Quinonez Silvero, N.R., de Sousa Mendes, W., Bonfatti, B.R., Dotto, A.C., Urbina Salazar, D.F., de Oliveira Mello, F.A., de Silveira Paiva, A.F., Barros Souza, A., dos Santos, N.V., Nascimento, C.M., de Mello, D.C., Bellinaso, H., Gonzaga Neto, L., Accorsi Amorim, M.T., de Resende, M.E.B., de Souza Vieira, J., de Queiroz, L.G., Gallo, B.C., Sayao, V.M., de Silva Lisboa C.J., 2020. Bare Earth's Surface Spectra as a Proxy for Soil Resource Monitoring. Scientific Reports, 10:4461.

Statistisches Bundesamt (Destatis), 2017. Land- und Forstwirtschaft, Fischerei. Methodische Grundlagen der Agrarstrukturerhebung 2016. Fachserie 3 Reihe 2. S.5. Published: 05/02/2017; Art.no.: 2032605169004.

Statistisches Bundesamt (Destatis), 2018. Data licence Germany – „1111-01-01-4 Gebietsfläche in qkm – Stichtag 31.12. – regionale Tiefe: Kreise und krfr. Städte" – Version 2.0 (licence text available at www.govdata.de/dl-de/by-2-0). Online: https://www.regionalstatistik.de/genesis/online/data;sid=720713C799CA2789F6A9C8153B7F0911.reg1?operation=abruftabelleBearbeiten&levelindex=2&levelid=1583486661043&auswahloperation=abruftabelleAuspraegungAuswaehlen&auswahlverzeichnis=ordnungsstruktur&auswahlziel=werteabruf&selectionname=11111-01-01-4&auswahltext=&werteabruf=Werteabruf (accessed July 2018).

Statistisches Bundesamt (Destatis), 2020 a. Data licence Germany – „41120-01-02-4-B landwirtschaftliche Betriebe & landwirtschaftlich genutzte Flächen (LF) nach Kulturarten Erhebungsjahr – regionale Ebene" – Version 2.0 (licence text abailable at www.govdata.de/dl-de/by-2-0). Online: https://www.regionalstatistik.de/genesis/online/data;sid=DBAD6FFC87187C0E7C135DE45AF1BA91.reg2?operation=abruftabelleAbrufen&selectionname=41120-01-02-4-B&levelindex=1&levelid=1580825413509&index=2 (accessed January 2020).

Statistisches Bundesamt (Destatis), 2020 b. Data licence Germany – „41141-01-01-4-B landwirtschaftliche Betriebe & landwirtschaftlich genutzte Fläche (LF) nach Kulturarten – Jahr – regionale Ebene" – Version 2.0 (licence text available at www.govdata.de/dl-de/by-2-0). Online: https://www.regionalstatistik.de/genesis/online/data;sid=063CCEEC3A73F6F691D924763E80A785.reg2?operation=abruftabelleAbrufen&selectionname=41141-01-01-4-B&levelindex=1&levelid=1580825429023&index=2 (accessed January 2020).

Diek, S., Fornallaz, F., Schaepman, M.E., de Jong, R., 2017. Barest Pixel Composite for Agricultural Areas Using Landsat Time Series. Remote Sensing, 2017, 9, 1245.

EEA, 2007. CLC 2006 technical guidelines. In: EEA Technical Report, No. 17/2007, Copenhagen. URL: https://www.eea.europa.eu/publications/technical_report_2007_17 (last access: 20.04.2020).

EEA, 2016. Biogeographic Regions in Europe. European Environment Agency, https://www.eea.europa.eu/data-and-maps/figures/biogeographical-regions-in-europe-2 (last access: 20.04.2020).

EEA, 2020. Europe's biodiversity – biogeographical regions and seas. European Environmental Agency, Report No 1/2002. URL: https://www.eea.europa.eu/publications/report_2002_0524_154909 (last access: 20.04.2020).

Estel, S., Kuemmerle, T., Levers, C., Baumann, M., Hostert, P., 2016. Mapping cropland-use intensity across Europe using MODIS NDVI time series. Environmental Research Letters, 11, 024015.

Flood, N., 2014. Continuity of Reflectance Data between Landsat-7 ETM+ and Landsat-8 OLI, for Both Top-of-Atmosphere and Surface Reflectance: A Study in the Australian Landscape. Remote Sensing, 6, 7952-7970.

Gobin, A., Jones, R., Kirkby, M., Campling, P., Govers, G., Kosmas, C., Gentile, A.R., 2004. Indicators for pan-European assessment and monitoring of soil erosion by water. Environmental Science & Policy, 7, 25-38.

Griffiths, P., Nendel, C., Hostert, P., 2019. Intra-annual reflectance composites from Sentinel-2 and Landsat for national-scale crop and land cover mapping. Remote Sensing of Environment, 220, 135-151.

Hansen, M.C., Egorov, A., Roy, D.P., Potapov, P., Ju, J., Turubanov, S., Kommareddy, I., Loveland, T.R., 2011. Continuous fields of land cover for the conterminous United States using Landsat data: first results from the Web-Enabled Landsat Data (WELD) project. Remote Sensing Letters, 2, 279-288.

Hermosilla, T., Wulder, M.A., White, J.C., Coops, N.C., Hobart, G.W., 2015. An integrated Landsat time series protocol for change detection and generation of annual gap-free surface reflectance composites. Remote Sensing of Environment, 158, 220-234.

Holden, C.E., Woodcock, C.E., 2016. An analysis of Landsat 7 and Landsat 8 underflight data and the implications for time series investigations. Remote Sensing of Environment, 185, 16-36.

Ienco, D., Interdonato, R., Gaetano, R., Minh, D.H.T., 2019. Combining Sentinel-1 and Sentinel-2 Satellite Image Time Series for land cover mapping via a multi-source deep learning architecture. ISPRS Journal of Photogrammetry and Remote Sensing, 158, 11-22.

Kleinbaum, D. Dietz, D.G., Gail, M., Klein, M., Klein, M. (2002). Logistic regression. New York Springer-Verlag.

Kovalskyy, V., Roy, D.P., 2013. The global availability of Landsat 5 TM and Landsat 7 ETM+ land surface observations and implifications for global 30 m Landsat data product generation. Remote Sensing of Environment, 130, 280-293.

Labriere, N., Locatelli, B., Laumonier, Y., Freycon, V., Bernoux, M. (2015). Soil erosion in the humid tropics: A systematic quantitative review. Agriculture, Ecosystems and Environment, 203, 127-139.

Lacroix, P., Bievre, G., Pathier, E., Kniess, U., Jongmans, D., 2018. Use of Sentinel-2 images for the detection of precursory motions before landslide failures. Remote Sensing of Environment, 215, 507-516.

Langford, R.L., 2015. Temporal merging of remote sensing data to enhance spectral regolith, lithological and alteration patterns for regional mineral exploration. Ore Geology Reviews, 68, 14-29.

Lavelle, P., Rodriguez, N., Arguello, O., Bernal, J., Botero, C., Chaparro, P., Gomez, Y., Guiterrez, A., del Pilar Hurtado, M., Loaiza, S, Pullido, S.X., Rodriguez, E., Sanabria, C., Velasquez, E., Fonte, S.J., 2014. Soil ecosystem services and land use in the rapidly changing Orinoco River Basin of Colombia. Agriculture, Ecosystems and Environment, 185, 106-117.

Li, S., Wang, W., Ganguly, S., Nemani, R., 2018. Radiometric Characteristics of the Landsat Collection 1 Dataset. Advances in Remote Sensing, 7, 203-217.

Lobell, D.B., Ortiz-Monasterio, J.I., Gurrola, F.C., Valenzula, L., 2007. Identification of saline soils with multiyear remote sensing of crop yields. Soil Science Society of America Journal, 7, 777-783.

Loiseau, T., Chen, S., Mulder, V.L., Roman Dobarco, M., Richer-de-Forges, A.C., Lehmann, S., Bourennane, H., Saby, N.P.A., Martin, M.P., Vaudour, E., Gomez, C., Lagacherie, P., Arrouays, D., 2019: Satellite data integration for soil caly content modelling at a national scale. International Journal of Applied Earth Observation and Geoinformation, 82, 101905.

Malec, S., Rogge, D., Heiden, U., Sanchez-Azofeifa, A., Bachmann, M., Wegmann, M., 2015. Capability of spaceborne hyperspectral EnMAP mission for mapping fractional cover for soil modeling. Remote Sensing, 7 (9), 11776-11800.

Markham, B.L., Storey, J.C., Williams, D.L., Irons, J.R., 2004. Landsat sensor performance: History and Current Status. IEEE Transactions on Geoscience and Remote Sensing, 42, 12, 2691-2694.

Okin, G.S., 2007. Relative spectral mixture analysis – A multitemporal index of total vegetation cover. Remote Sensing of Environment, 106, 467-479.

Panagos, P., Karydas, C., Borelli, P., Ballabio, C., Meusburger, K., 2014 a. Advances in soil erosion modelling through remote sensing availability at European scale. Proc. SPIE 9229, Second International Conference on Remote Sensing and Geoinformation of the Environment (RSCy2014), 92290I (12 August 2014).

Panagos, P., Meusburger, K., van Liedekerke, M., Alewell, C., Hiederer, R., Montanarella, L., 2014 b. Assessing soil erosion in Europe based on data collected through a European network. In: Soil Science and Plant Nutrition, 60:1, 15-29; DOI: 10.1080/00380768.2013.835701.

Panagos, P., Borelli, P., Meusburger, K., 2015. A New European Slope Length and Steepness Factor (LS-Factor) for Mideling Soil Erosion by Water. In: Geoscience, 5, 117-126; DOI: 10.3390/geosciences5020117.

Pimentel, D., Burgess, M. (2013). Soil Erosion Threatens Food Production. Agriculture, 3, 443-463.

Richards, J.A. 1993. Remote Sensing Digital Image Analysis: An Introduction, 2nd ed. Berlin: Springer-Verlag.

Richter. R., Schläpfer, D., Müller, A., 2006. An automatic atmospheric correction algorithm for visible/NIR imagery. International Journal of Remote Sensing, 27:10, 2077-2085; DOI: 10.1080/01431160500486690.

Richter, R., 2010. Atmospheric/topographical correction for airborne imagery. ATCOR4 User Guide. Wessling, Germany.

Richter, R., Schläpfer, D., 2014. Atmospheric / Topographic Correction for Satellite Imagery (ATCOR-2/3 User Guide, Version 8.3. 1, February 2014). ReSe Applications Schläpfer Langeggweg 3.

Rogge, D., Bauer, A., Zeidler, J., Müller, A., Esch, T., Heiden, U., 2018. Building an exposed soil composite processor (SCMaP) for mapping spatial and temporal characteristics of soils with Landsat imagery (1984-2017). Remote Sensing of Environment, 205, 1-17.

Rouse, J.W., Haas, R.H., Schell, J.A., Deering, D.W., 1974. Monitoring Vegetation Systems in the Great Plains with ERTS Proceesing. Proceedings of the Third Earth Reserves Technology Satellite Symposium, Greenbelt: NASA SP-351, 1974, Vol. 30103017.

Roy, D.P., Kovalskyy, V., Zhang, H.K., Vermote, E.F., Yan, L., Kumar, S.S., Egorov E., 2016. Characterization of Landsat-7 to Landsat-8 reflective wavelength and normalized difference vegetation index continuity. Remote Sensing of Environment, 185, 57-70.

Schmidt, S., Meusburger, K., de Figueiredo, T., Alewell, C., 2017. Modelling Hot Spots of Soil Loss by Wind Erosion (SoLo Wind) in Western Saxony, Germany. Land Degradation & Development, 28, 1100-1112.

Steinhoff-Knopp, B., Burkhard, B., 2018. Soil erosion by water in Northern Germany: long-term monitoring results from Lower Saxony. Catena, 165 (2018), 299-309.

Teillet, P.M., Barker, J.L., Markham, B.L., Irish, R.R., Fedosejevs, G., Storey, J.C., 2001. Radiometric cross-calibration of the Landsat-7 ETM+ and Landsat-5 TM sensors based on tamdem data sets. Remote Sensing of Environment, 78, 39-54.

Thonfeld, F., Steinebach, S., Muro, J., Kirmi, F., 2020. Long-Term Land Use/Land Cover Change Assessment of the Kilombero Catchment in Tanzania Using Random Forest Classification and Robust Change Vector Analysis. Remote Sensing, 12, 1057.

Toffoli, T., Margolous, N., 1987. Cellular Automata Machines: A New Environment for Modeling. MIT Press: Cambridge, MA, USA, 1987; ISBN 0-262-20060-0.

USGS, 2020. Landsat Mission – Landsat Level-1 Processing Details. United States Geological Suvey. URL: https://www.usgs.gov/land-resources/nli/landsat/landsat-level-1-processing-details (last access: 20.04.2020).

Vaudour, E., Gomez, C., Lagacherie, P., Loiseau, T., Baghdadi, N., Urbina-Salazar, D., Loubet, B., Arrouays, D. (2021): Temporal mosaicking approaches of Sentinel-2 images for extending topsoil organic carbon content mapping in croplands. International Journal of Applied Earth Observations and Geoinformation, 96, 102277.

Virto, I., Jose Imaz M., Fernandez-Ugalde, O., Gartzia-Begngoetxea, N., Enrique, A., Bescansa, P., 2015. Soil Degradation and Soil Quality in Western Europe: Current Situation and Future Perspectives. In: Sustainability, 7, 313-365; DOI: 10.3390/su7010313.

White, J.C., Wulder, M.A., Hobart, G.W., Luther, J.E., Hermosilla, T., Griffiths, P., Coops, N.C., Hall, R.J., Hostert, P., Dyk, A., Guindon, L., 2014. Pixel-Based Image Compositing for Large-Area Dense Time Series Applications and Science. Canadian Journal of Remote Sensing, 40:3, 192-212.

Wulder, M.A., Loveland, T.R., Roy, D.P., Crawford, J.C., Masek, J.G., Woodcock, C.E., Allen, R.G., Anderson, M.C., Belward, A.S., Cohen, W.B., Dwyer, J., Erb, A., Gao, F., Griffiths, P., Helder, D. Hermosilla, T., Hipple, J.D., Hostert, P., Hughes, M.J., Huntington, J., Johnson, D.M., Kennedy, R., Kilic, A., Li, Z., Lymburner, L., McCorkel, J., Pahlevan, N., Scambos, T.A., Schaaf, C., Schott, J.R., Sheng, Y., Storey, J., Vermote, E., Vogelmann, J., White, J.C., Wynne, R.H., Zhu, Z., 2019. Current status of Landsat program, science and applications. Remote Sensing of Environment, 225, 127-147.

Xu, D., Guo, X. 2014. Compare NDVI extracted from Landsat 8 imagery with that from Landsat 7 imagery. American Journal of Remote Sensing, 2014;2(2): 10-14.

Ying, Q., Tyukavina, A., Wang, L., Hansen, M.C., Hancher, M., Popatov, P.V., Moore, R., Stehman, S.V. 2017. Global bare ground gain from 2000 to 2012 using Landsat imagery. Remote Sensing of Environment, 194, 161-176.

Zhao, D., Jiang, H., Yang, T., Cai, Y., Xu, D., Shuqing, A., 2012. Remote sensing of aquatic vgetation distribution in Taihu Lake using an improved classification tree with modified thresholds. Journal of Environmental Management, 95, 98-107.

Zhu, Z., Woodcock, C.E. 2012. Object-based cloud and cloud shadow detection in Landsat imagery. Remote Sensing of Environment 118 (15), 89-94.

Zhu, Z., Wang, S., Woodcock, C.E., 2015. Improvement and expansion of the Fmask algorithm: cloud, cloud shadow, and snow detection for Landsats 4-7, 8 and Sentinel-2 images. Remote Sensing of Environment, 159, 269-277.

Zhu, Z., Fu, Y., Woodcock, C.E., Olofsson, P., Vogelmann, J.E., Holden, C., Wang, M., Dai, S., Yu, Y., 2016. Including land cover change in analysis of greenness trends using all available Landsat 5, 7 and 8 images: A case study from Guangzhou, China (2000-2014). Remote Sensing of Environment, 185, 243-257.

Zhuo, L. Dai, Q., Hand, D., Chen, N., Zhao, B., Berti, M., 2018. Evaluation of remotely sensed soil moisture for landslide hazard assessment. IEEE Journal of Selected Topics in Applied Earth Observations and Remote Sensing, 12, 1, 162-173.